

A COMPUTATIONAL STUDY OF AERODYNAMICS
OF A TILTED WEB OVER AN AIR REVERSER

By

HALLOLUWA K. S. JAYASEKARA

Bachelor of Science

Oklahoma State University

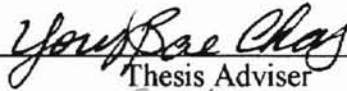
Stillwater, Oklahoma

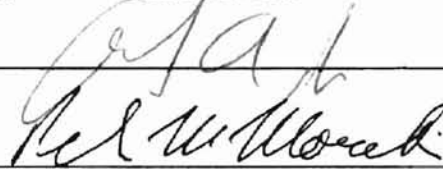
1999

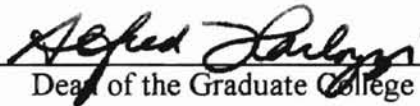
Submitted to the Faculty of the
Graduate College of the
Oklahoma State University
in partial fulfillment of
the requirements for
the Degree of
MASTER OF SCIENCE
December, 2000

A COMPUTATIONAL STUDY OF AERODYNAMICS
OF A TILTED WEB OVER AN AIR REVERSER

Thesis Approved:


Thesis Adviser


Chair


Dean of the Graduate College

ACKNOWLEDGEMENTS

I would first and foremost wish to express my thanks and appreciation to my advisor, Dr. Young Chang, for his patience, constructive guidance, and his dedication to the field of teaching and research. I would also like to express my thanks to my other committee members, Dr. Andy Arena, Jr. and Dr. Peter Moretti, for their guidance. I would like to take time to thank all my friends for their support throughout the years. I would like to give a special thanks to Lyon Hong for all the help and encouragement given during the phase of this research.

Many thanks to my parents for their support and guidance. I would also like to express my thanks to my husband for his unending patience and love and especially for being a very good friend and a partner. The very special thanks to my grandmother, my uncle Kumara Jyasuriya and my aunt Salmi Jayasuriya for their encouragement when I needed it the most.

I would like to thank all the Mechanical Engineering faculty and staff members for their support throughout the years and for all the opportunities that they provided for me to learn both in and out of the classroom. Finally, I would like to thank Web Handling Research Center (WHRC) at Oklahoma State University and its consortium member companies for supporting me during the course of this research.

TABLE OF CONTENTS

CHAPTER	Page
I. INTRODUCTION.....	1
1.1 Background	1
1.2 Research Objectives	2
II. LITERATURE REVIEW.....	3
III. COMPUTATIONAL MODELING OF WEB OVER AN AIR REVERSER.....	5
3.1 Description of Computational Model.....	5
3.1.1 Modeling of Air Holes	6
3.2 Computational Model.....	8
3.3 Validity of the Computational Model	10
3.3.1 Grid.....	10
3.3.2 Skewness	11
3.3.3 Viscous Model.....	11
3.4 Procedure of Computational Modeling.....	13
IV. COMPUTATIONAL RESULTS.....	15
4.1 Non-Tilted Web.....	16
4.2 Tilted Web.....	22
4.2.1 Static Pressure Distribution	22
4.2.2 Shear Stress Distribution	27
4.2.3 Lift Force	29
4.2.4 Lateral Forces	31
4.2.4 Discharge Coefficient.....	34
4.3 Comparison with Analytical Results.....	36
4.3.1 Pressure Distribution	37
4.3.2 Lift Force and Lateral Force.....	39

V. CONCLUSIONS.....	45
VI. RECOMMENDATIONS FOR FUTURE STUDY	46
REFERANCES.....	46

LIST OF FIGURES

Figure 1. Schematic View of a Web Over an Air Reverser	2
Figure 2. Computational Model	6
Figure 3. Air-Emitting Holes on an Air Reverser	6
Figure 4. Modeling of Equivalent Slot Width.....	7
Figure 5. Schematic of Computational Domain.....	8
Figure 6. Dimensions of the Computational Model	9
Figure 7. Comparison of Two Different Turbulence Models	12
Figure 8. Grid Around the Slot for Non-Tilted Web ($h_c = 10$ mm)	15
Figure 9. Velocity Contours near the Left Edge ($h_c = 4$ mm and $\beta = 0$ deg)	16
Figure 10. Velocity Contours in the Central Region ($h_c = 4$ mm and $\beta = 0$ deg).....	17
Figure 11. Velocity Contours near the Right Edge ($h_c = 4$ mm and $\beta = 0$ deg).....	17
Figure 12. Velocity Contours near the Left Edge ($h_c = 10$ mm and $\beta = 0$ deg).....	18
Figure 13. Velocity Contours in the Central Region ($h_c = 10$ mm and $\beta = 0$ deg).....	18
Figure 14. Velocity Contours near the Right Edge ($h_c = 10$ mm and $\beta = 0$ deg).....	19
Figure 15. Effect of Flotation Height on Static Pressure Distribution on the Web.....	19

Figure 16. Effect of Flotation Height on Shear Stress	21
Figure 17. Effect of Flotation Height on Lift Force	21
Figure 18. Effect of Tilt Angle on Pressure Distribution on the Web ($h_c = 4$ mm)	22
Figure 19. Effect of Tilt Angle on Pressure Distribution on the Web ($h_c = 6$ mm)	23
Figure 20. Effect of Tilt Angle on Pressure Distribution on the Web ($h_c = 8$ mm)	23
Figure 21. Effect of Tilt Angle on Pressure Distribution on the Web ($h_c = 10$ mm)	24
Figure 22. Velocity Contours near the Left Edge ($h_c = 4$ mm and $\beta = 0.50$ deg)	25
Figure 23. Velocity Contours near the Right Edge ($h_c = 4$ mm and $\beta = 0.50$ deg)	25
Figure 24. Velocity Contours near the Left Edge ($h_c = 10$ mm and $\beta = 1.00$ deg)	26
Figure 25. Velocity Contours near the Right Edge ($h_c = 10$ mm and $\beta = 1.00$ deg)	26
Figure 26. Effect of Tilt Angle on Shear Stress ($h_c = 4$ mm)	27
Figure 27. Effect of Tilt Angle on Shear Stress ($h_c = 6$ mm)	28
Figure 28. Effect of Tilt Angle on Shear Stress ($h_c = 8$ mm)	28
Figure 29. Effect of Tilt Angle on Shear Stress ($h_c = 10$ mm)	29
Figure 30. Effect of Tilt Angle on Lift Force	30
Figure 31. Effect of Tilt Angle on Lift Force Ratio	30
Figure 32. Effect of Tilt Angle on the Lateral Force ($h_c = 4$ mm)	32

Figure 33. Effect of Tilt Angle on the Lateral Force ($h_c = 6$ mm)	32
Figure 34. Effect of Tilt Angle on the Lateral Force ($h_c = 8$ mm)	33
Figure 35. Effect of Tilt Angle on the Lateral Force ($h_c = 10$ mm)	33
Figure 36. Lateral Aerodynamic Force on Tilted Web	34
Figure 37. Variation of Discharge Coefficient.....	36
Figure 38. Comparison of Pressure Profiles for $h_c = 4$ mm	37
Figure 39. Comparison of Pressure Profiles for $h_c = 6$ mm	38
Figure 40. Comparison of Pressure Profiles for $h_c = 8$ mm	38
Figure 41. Comparison of Pressure Profiles for $h_c = 10$ mm	39
Figure 42. Comparison of Lift Forces for $\beta = 0.00$ deg	40
Figure 43. Comparison of Lateral Forces for $h_c = 4$ mm	40
Figure 44. Comparison of Lateral Forces for $h_c = 6$ mm	41
Figure 45. Comparison of Lateral Forces for $h_c = 8$ mm	41
Figure 46. Comparison of Lateral Forces for $h_c = 10$ mm	42
Figure 47. Comparison of Pressure Profiles for $h_c = 4$ mm and $C = 0.801$	43
Figure 48. Comparison of Pressure Profiles for $h_c = 6$ mm and $C = 0.840$	43
Figure 49. Comparison of Pressure Profiles for $h_c = 8$ mm and $C = 0.875$	44

Figure 50. Comparison of Pressure Profiles for $h_c = 10$ mm and $C = 0.839$ 44

LIST OF TABLES

Table 1. Conditions of Calculation	10
Table 2. Values of Variables Used to Determine Discharge Coefficient	35

NOMENCLATURE

b	Width of slot
C	Discharge coefficient
d	Diameter of air-emitting holes
F_y	Lateral aerodynamic force on a tilted web per unit length
$F_{y(\text{due to friction})}$	Lateral aerodynamic force on a tilted web per unit length due to friction
$F_{y(\text{due to pressure})}$	Lateral aerodynamic force on a tilted web per unit length due to pressure
h_c	Average flotation height
L	Lift force per unit length of web
p_o	Gage pressure inside the air reverser
Q_{hole}	Mass flow rate through the air holes
Q_{slot}	Mass flow rate through the slots
R	Radius of air reverser
S_{CD}	Cross-direction pitch of holes and slots
S_{MD}	Machine-direction pitch of air-emitting holes
W	Width of web

α	$\sqrt{2} Cb/HS_{CD}$
β	Tilt angle
Δp	Pressure difference across the air reverser wall
ρ	Density of air
τ_{web}	Cross-direction shear stress on the web surface

CHAPTER 1

INTRODUCTION

1.1 Background

Continuous, strip-formed, flexible materials such as paper, metal foils and polymer films are called webs. When wet coated webs are transported, the wet surface cannot be touched until they are dry. Some materials such as adhesive tapes and magnetic media must be handled with extreme care. One way of supporting web materials without contact is to use devices called air reversers or airturn bars.

This research focuses on one type of air reversers that are hollow, cylindrical, porous drums. Figure 1 represents the schematic of a web over such an air reverser. The web floats over an air cushion formed between the web and the reverser, which emits air through multiple holes. A web line is equipped with a tension control mechanism, which maintains a constant web tension throughout the process. Web tension and the turning radius determine the cushion pressure or pull down pressure. Cushion pressure is proportional to web tension and inversely proportional to turning radius. The steady state air pressure in the interface is related to clearance between the web and the air reverser surface. When the air is injected into the clearance, it causes the web to deflect from its initial state; which causes variation of the air pressure. Therefore, the aerodynamics is coupled with the deflection of the web and vice versa.

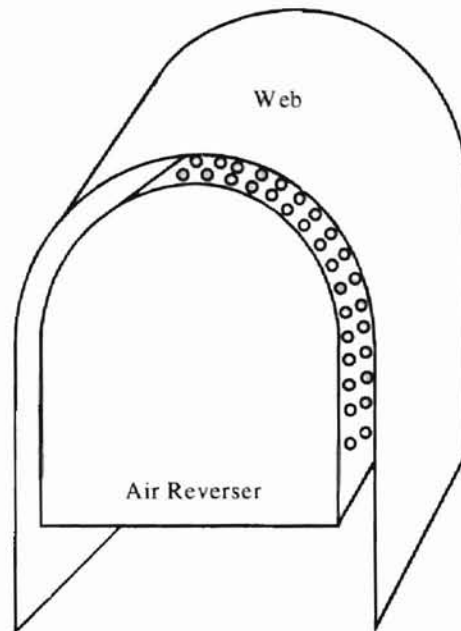


Figure 1. Schematic View of a Web Over an Air Reverser

1.2 Research Objectives

The primary objective of this study is to analyze the effect of tilt angle of the web on the aerodynamics of air reversers. The following aerodynamic effects are considered:

- Pressure profile on a tilted web supported by an air reverser.
- Lateral aerodynamic force on a tiled web due pressure loads.
- Lateral force due to air friction.

CHAPTER 2

LITERATURE REVIEW

The fundamentals of the lateral behavior of a moving web were established by Shelton (1968, 1971a, 1971b). He analyzed the static and dynamic behavior of a moving web supported by rollers. The main assumption in his analytical model is that the web is initially straight.

Rogen (1990) analyzed the subject of wrapping of a thin web over a cylindrical drum, including large wrap angles. He used Donnell's (1976) theory to model the web deflection. Donnell's theory is an extension of von Karman's plate theory. Lin and Mote (1995,1996) used von karman's plate theory to study buckling of a flat web in the free span between two rollers.

Sundaram and Benson (1989) and Muftu and Benson (1995) used the small deflection cylindrical shell theory to study dynamic effects in the web wrapping over a cylindrical structure. Muftu and Cole (1999) studied the aerodynamics of a web supported by a cylindrical air reverser. In that paper, web deflections were modeled by a moderately large deflection "cylindrical" shell theory with a continuous curvature variation and a self-adjusting reference state, near the steady state of the web. This approach yields an efficient method to obtained deflection history of the web. Barlow (1967) first introduced the self-adjusting reference state in connection with the analysis of flexible tapes.

Benson and D'Errico (1991, 1993) analyzed interfacial mechanics of a web wrapping around a bumpy drum considering adjustable reference radius. In their model, an initially unknown reference radius is defined where the in plane stresses vanish. They analyzed only the circumferentially symmetric case. Benson (1998) analyzed the static equilibrium of a long elastic tape wrapping onto a rigid drum. Strains are assumed to be small but rotations of the beam are assumed to be large. The nonlinear theory of the elastica (Frisch-Fay, 1962) is used to model the small-strain, large-rotation, quasi-static deformation of the tape.

Wolfshtein (1970) analyzed the problem of turbulent jet impinging vertically to a horizontal surface. He used iterative finite-difference method to obtain solutions to the turbulent impinging jet. The static pressure distribution on the wall shows a peak point around the stagnation point. As the jet moves along the wall, the pressure approaches the ambient pressure. The skin friction and jet velocity along the wall also follow the similar trend to the pressure. The jet velocity and skin friction are zero at the stagnation point, but they become maximum at a certain distance from the stagnation point and then decrease. Hwang and Liu (1989) performed a numerical study on the impinging jet. Their model is similar to Wolfshtein's. The only difference is that Hwang and Liu placed a flat wall above the jet nozzle. Their numerical results show similar trend to the Wolfshtein's. They also analyzed the effect of two surfaces on the static pressure. It is shown that as the distance reduces, the static pressure at the stagnation point increases while the pressures on both sides of the stagnation point reduce.

CHAPTER 3

COMPUTATIONAL MODELING OF WEB OVER AN AIR REVERSER

Computational modeling for a tilted, rigid, stationary web over an air reverser is presented and discussed in this chapter. The computational results obtained by FLUENT include the effects of tilt angle and average flotation height on the aerodynamic forces on the web over an air reverser.

3.1 Description of Computational Model

The following assumptions are introduced:

- 1) The web is stationary, rigid, and flat.
- 2) The web has infinite length but finite width.
- 3) The flow is two-dimensional, steady, viscous and compressible.

With the above assumptions, the air-emitting holes on the air reverser were replaced by equivalent slots with the same pitch in cross direction. Modeling of air holes is described in the section 3.1.1. Figure 2 represents computational model for the tilted web over an air reverser.

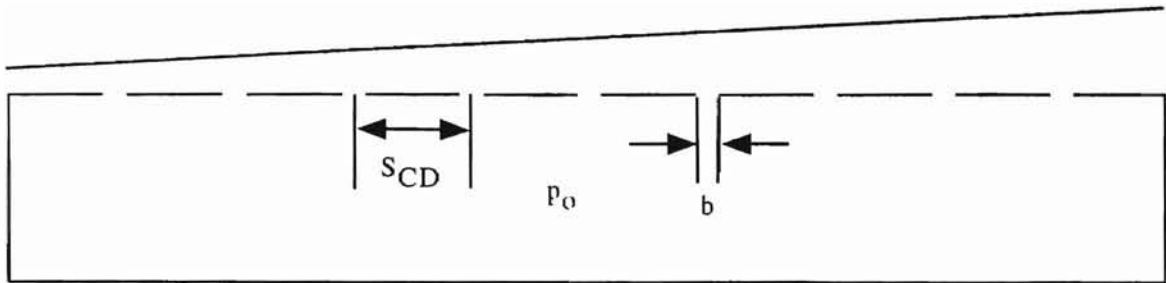


Figure 2. Computational Model

3.1.1 Modeling of Air Holes

Figure 3 shows the air holes on an actual air reverser. In the computational model, air holes are modeled as slots with finite width and infinite length in the machine direction. The distance between adjacent slots is the same as the distance between two adjacent holes in cross machine direction. The equivalent slot width is determined in such a way that the slots would yield the same open area as the holes per unit surface area. Figure 4 represents the schematic of equivalent slot width.

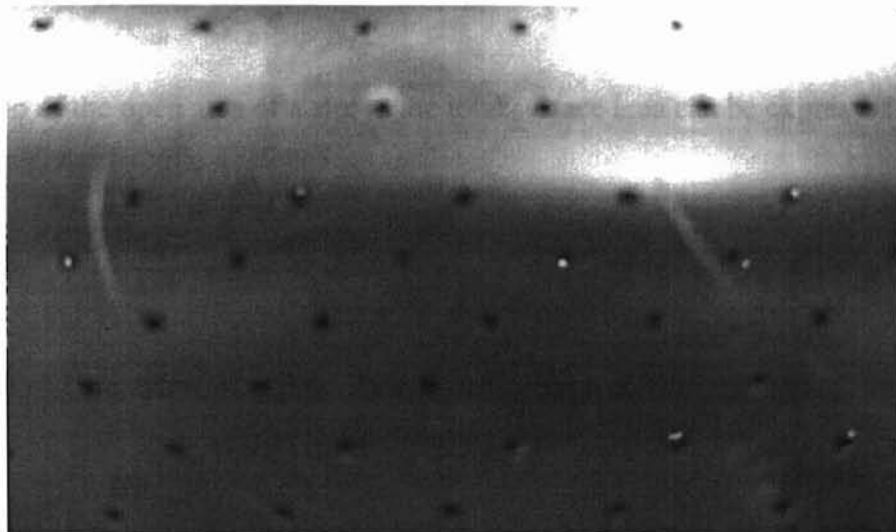


Figure 3. Air-Emitting Holes on an Air Reverser

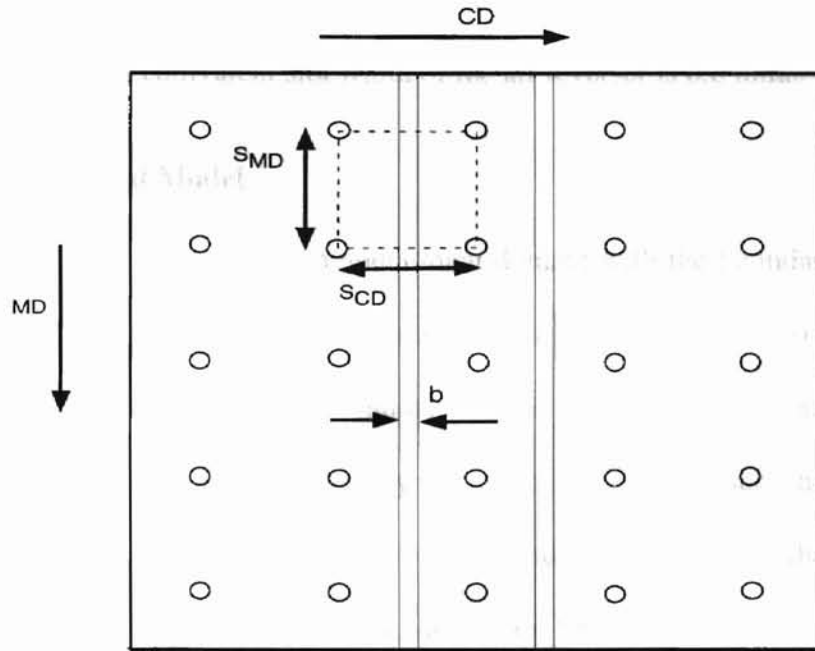


Figure 4. Modeling of Equivalent Slot Width

The ratio of the open area of the holes to the total surface area can be expressed as

$$\frac{A_{hole}}{A_{total}} = \frac{\frac{\pi}{4}d^2}{S_{CD}S_{MD}} \quad (1)$$

The ratio of the open area of a slot to the total surface area can be expressed as

$$\frac{A_{slot}}{A_{total}} = \frac{bS_{MD}}{S_{CD}S_{MD}} \quad (2)$$

Equating equations (1) and (2) yields the expression for equivalent slot width as a function of hole diameter and machine-directional pitch. The equivalent slot width is

$$b = \frac{\pi d^2}{4S_{MD}} \quad (3)$$

where d is the diameter of the hole. The diameter of the hole in this particular air reverser is 3.81 mm (0.15 inches) and the machine-direction pitch is 19.1 mm (0.75 inches), so that the equivalent slot width of the air reverser is 0.6 mm.

3.2 Computational Model

Figure 5 represents the computational domain with the boundary conditions. The computational domain consists of three different boundary conditions including wall, pressure inlet, and pressure outlet boundaries. The size of computational domain depends on how far the pressure outlet boundary is located from the pressure inlet boundary. The pressure at the inlet boundary is set to be the supply pressure to the system, and the pressure at the outlet boundary is assumed to be the ambient pressure (zero gage pressure). All walls are assumed smooth. This particular air reverser consists of counter-sunk sharp-edged holes, and the thickness of the air reverser wall and the hole diameter are in the same order of magnitude. Therefore, the holes are modeled as sharp-edged slot nozzles with an angle of 45 degrees.

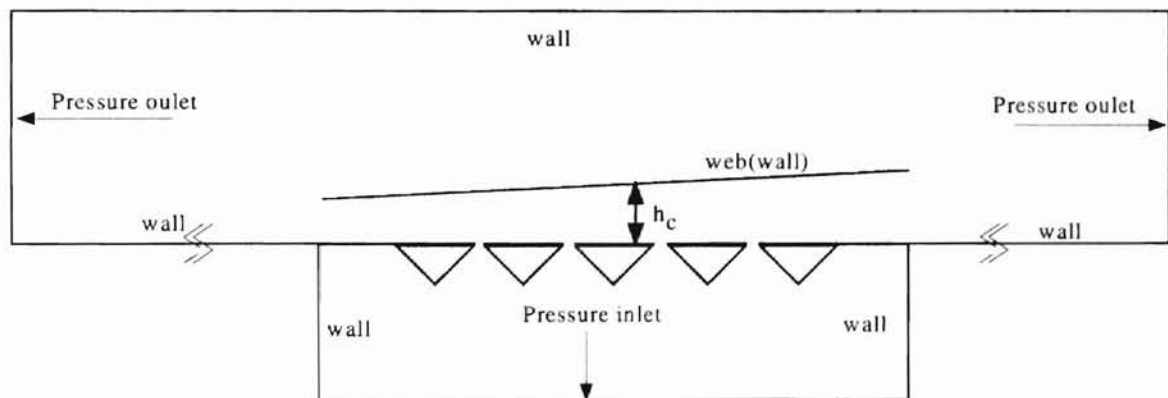


Figure 5. Schematic of Computational Domain

Table 1 lists the values of the major variables. The slot width and the width of web were not changed this study.

Table 1. Conditions of Calculation

h_c (mm)	Tilt Angle, β (deg)				
4	0.00	0.25	0.50	-	-
6	0.00	0.25	0.50	0.75	-
8	0.00	0.25	0.50	0.75	1.00
10	0.00	0.25	0.50	0.75	1.00

3.3 Validity of the Computational Model

In order to obtain correct solutions, several factors, which can affect numerical stability and accuracy of the solution, are considered.

3.3.1 Grid

Grid type must be compatible with the geometry because it must represent the behavior of the flow field throughout the model. The triangular grid, which is a type of unstructured grid, is used. Unstructured cells can be very fine in the high gradient zone and around very complex geometry. Cells may be coarse in the other areas. Mesh refinement can be done using the "Adapt" menu of FLUENT. Therefore, triangular meshes have geometric flexibility. In order to capture details of flow near slots more refined grids are used there. In order to obtain reasonably detailed results near the web, 800 nodes were placed along the web.

The main disadvantage of unstructured grid is that it may lead to an increase in numerical diffusion because the flow is not being aligned with the grid. Numerical diffusion occurs due to truncation errors during a computation. In order to reduce the

effects of the numerical diffusion on the solution, the second-order discretization scheme can be used. The second-order discretization scheme is given under the “Solve” menu of FLUENT.

3.3.2 Skewness

Another way to enhance the accuracy and the stability of the solution is to reduce the skewness of the grid. The skewness is defined as the difference between the shape of a cell and that of an equilateral cell with equivalent volume. The FLUENT manual suggests to keep the average skewness less than 0.5.

3.3.3 Viscous Model

The structure of turbulent boundary layer flow is very complex, random, and irregular. A correct selection of viscous model is very important. Several turbulence models such as Reynolds Stress Model (RSM) and k - ϵ model are available in FLUENT. The k - ϵ model is recommended for applications such as fully developed pipe flow, where fluid flow does not undergo sudden changes. According to Tannehill, Anderson, and Pletcher (1997), the Reynolds Stress Model yields more accurate results than the other models for flows with sudden changes in the mean strain rate. Figure 7 represents the static pressure profile on a non-tilted web obtained by using two different turbulence models. The ripples in the pressure are due to the impingement of air jets.

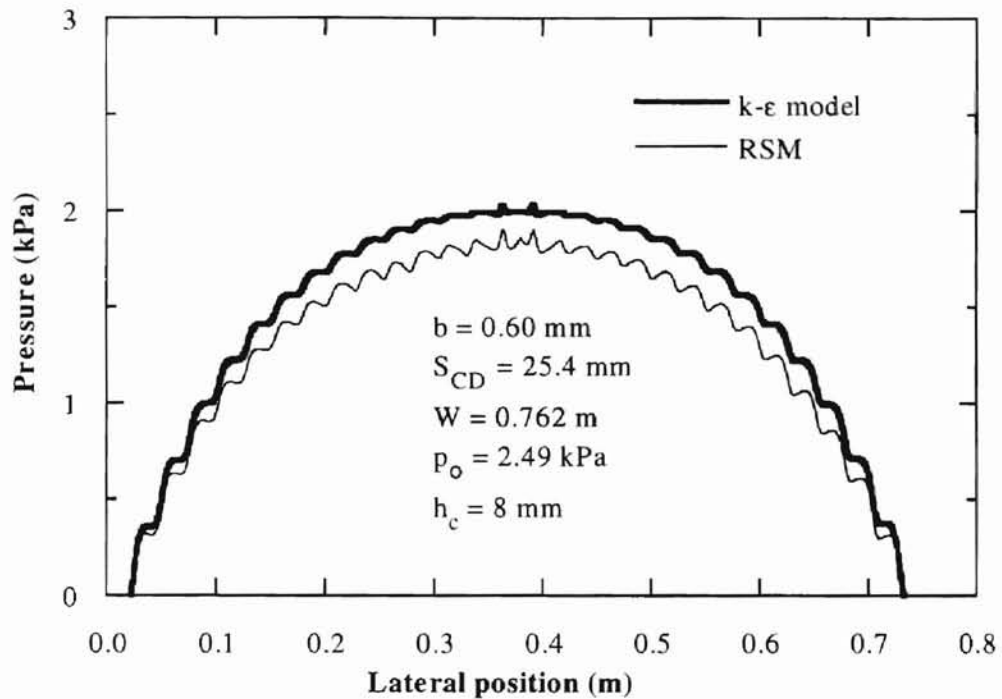


Figure 7. Comparison of Two Different Turbulence Models

It is seen that, the $k-\epsilon$ model predicts higher static pressure on the web than the Reynolds Stress Model. The Reynolds Stress Model or stress-equation model is mainly used in this study. This model is recommended for accurate analysis of turbulent flows, especially in near wall regions. On the other hand, Reynolds Stress Model has more numerical complexity than the $k-\epsilon$ model, because it does not assume that the turbulent shear stress is proportional to the eddy viscosity (Boussinesq assumption). The Reynolds Stress Model is more prone to diverge than the $k-\epsilon$ model. Reducing the relaxation factors or changing initial conditions can help overcome this problem. A viscous model can be selected under the “Define” menu and the sub menu of “Model”. In order to successfully solve the flow in near-wall regions, non-equilibrium wall functions are

selected. The non-equilibrium wall functions are recommended for the flows which undergo large pressure gradients and rapid change of the mean flow.

Properties of the fluid such as density and viscosity must be selected under the “Material” menu, and the initial values and boundary conditions must be specified. The air is assumed as ideal gas. All the material properties are evaluated at 300 K. The solution convergence criterion is set to be 1×10^{-5} in advance. The residuals convergence of continuity, x and y velocities, energy, and stresses are monitored until the convergence criterion is satisfied or until the static pressure acting on the web stops changing.

3.4 Procedure of Computational Modeling

GAMBIT is used to create a suitable computational domain, and FLUENT is used to solve the fluid dynamics. Modeling starts using GAMBIT, which is used to accomplish the following steps:

- 1) Create the geometry of the computational model.
- 2) Discretize the computational domain using an appropriate grid type.
- 3) Specify appropriate boundary conditions.
- 4) Export the generated mesh to be used by FLUENT.

Then use FLUENT to do the remaining tasks as follows:

- 1) Select an appropriate space formation (two-dimension or three-dimension).
- 2) Read the case file (exported mesh file).
- 3) Check the grid.
- 4) Convert units if necessary.
- 5) Check and smooth/swap grids.

- 6) Select a suitable turbulence model.
- 7) Select material properties.
- 8) Initialize the flow domain.
- 9) Specify boundary conditions.
- 10) Specify solution parameters.
- 11) Set convergence criterion.
- 12) Solve the flow domain.
- 13) Monitor residuals.
- 14) Use adaption if necessary.
- 15) Export the results.

CHAPTER 4

COMPUTATIONAL RESULTS

Computational results are presented and discussed in this chapter. In order to obtain accurate computational results, the grid should adequately represent the flow field. Therefore, prior to investigating computational results, the grids generated in the computational domain are examined. Figure 8 represents the grid generated for the case of a non-tilted web ($h_c = 10$ mm). In order to capture the details of the flow, the grid should be fine near the slots and along the web.

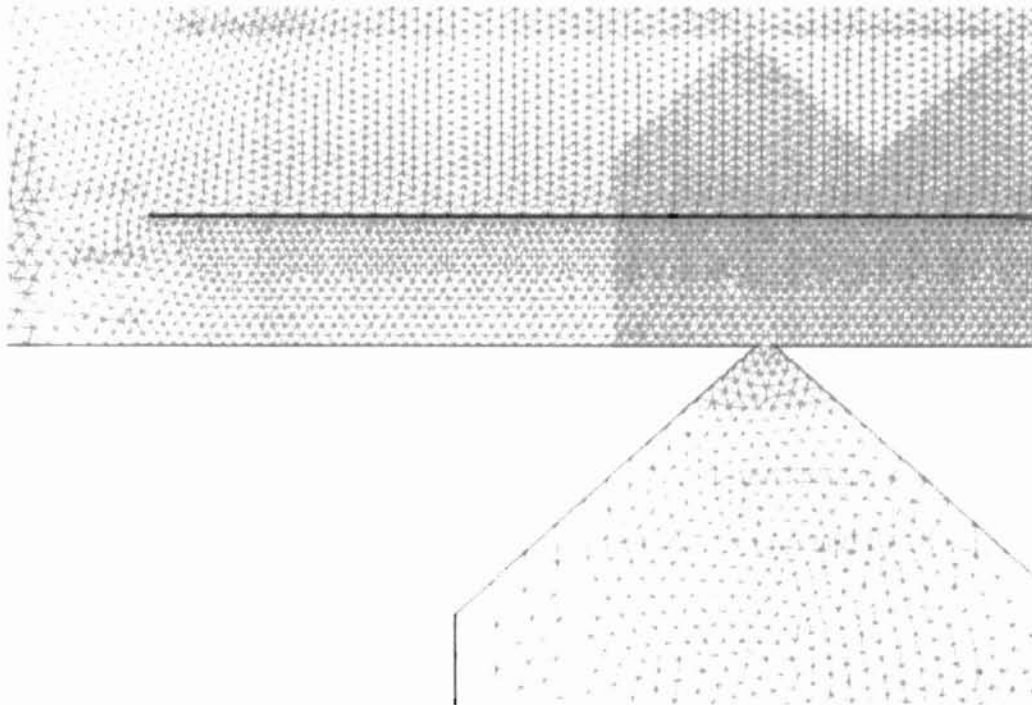


Figure 8. Grid Around the Slot for Non-Tilted Web ($h_c = 10$ mm)

4.1 Non-Tilted Web

The aerodynamics for a non-tilted web is examined first. Main variables and their ranges are listed in Table 1. The average flotation height is varied in the range of 4 mm to 10 mm. Figures 9 through 11 represent the contours of velocity near the left edge, middle region and the right edge, respectively, for $h_c = 4$ mm. Figures 12 through 14 represent the contours of velocity near the left edge, the center region, and the right edge, respectively, for $h_c = 10$ mm.

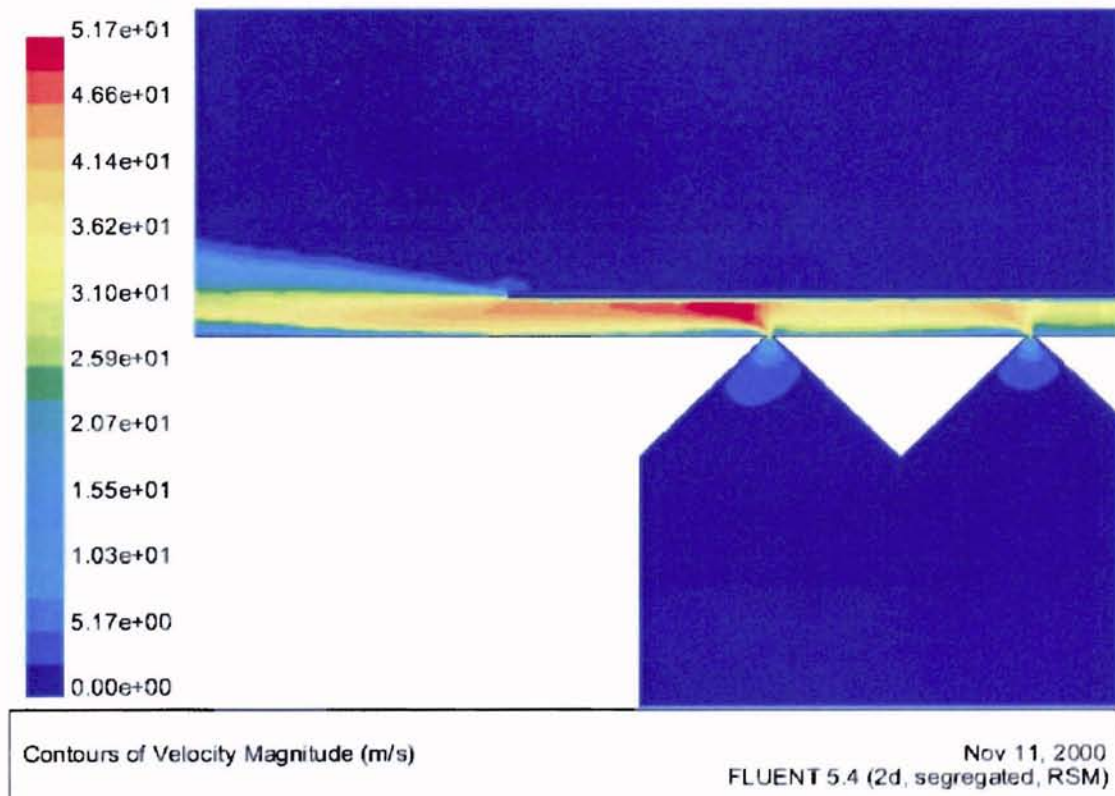


Figure 9. Velocity Contours near the Left Edge ($h_c = 4$ mm and $\beta = 0$ deg)

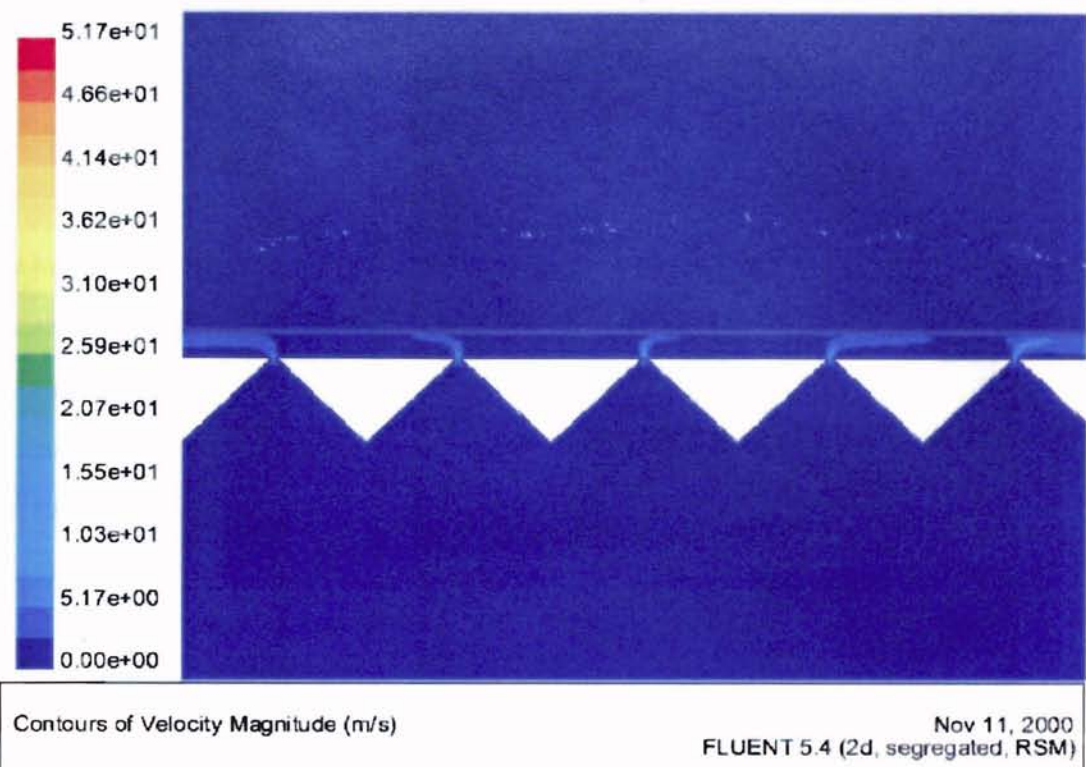


Figure 10. Velocity Contours in the Central Region ($h_c = 4$ mm and $\beta = 0$ deg)

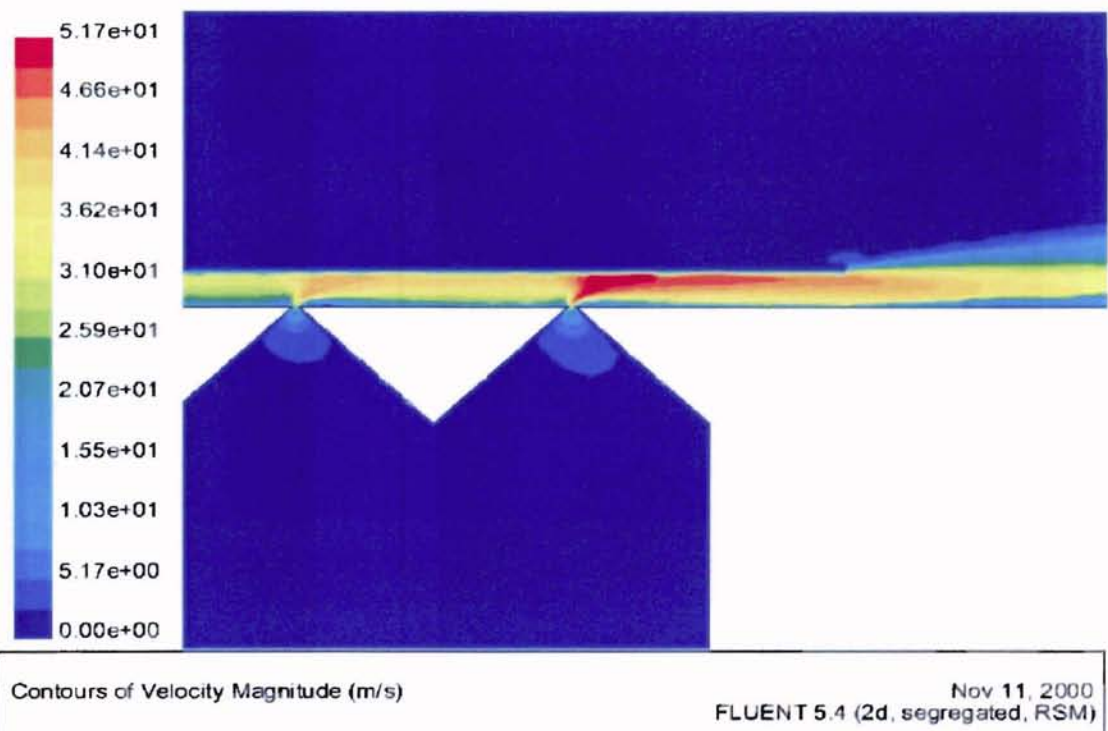


Figure 11. Velocity Contours near the Right Edge ($h_c = 4$ mm and $\beta = 0$ deg)

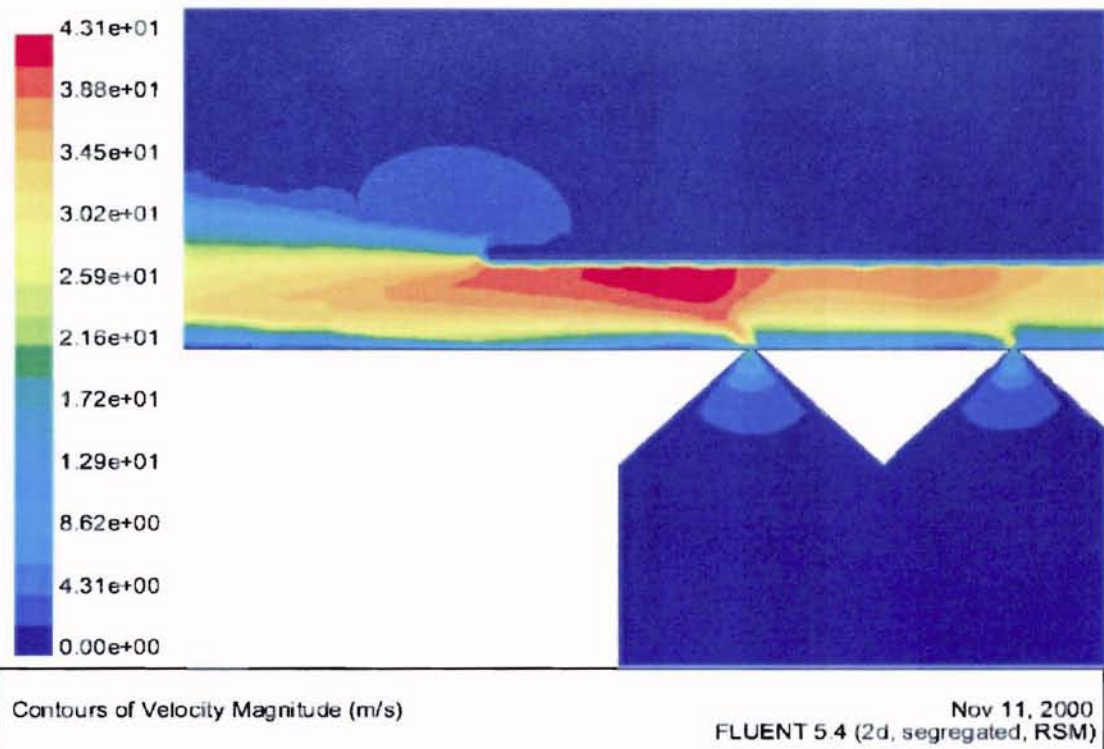


Figure 12. Velocity Contours near the Left Edge ($h_c = 10$ mm and $\beta = 0$ deg)

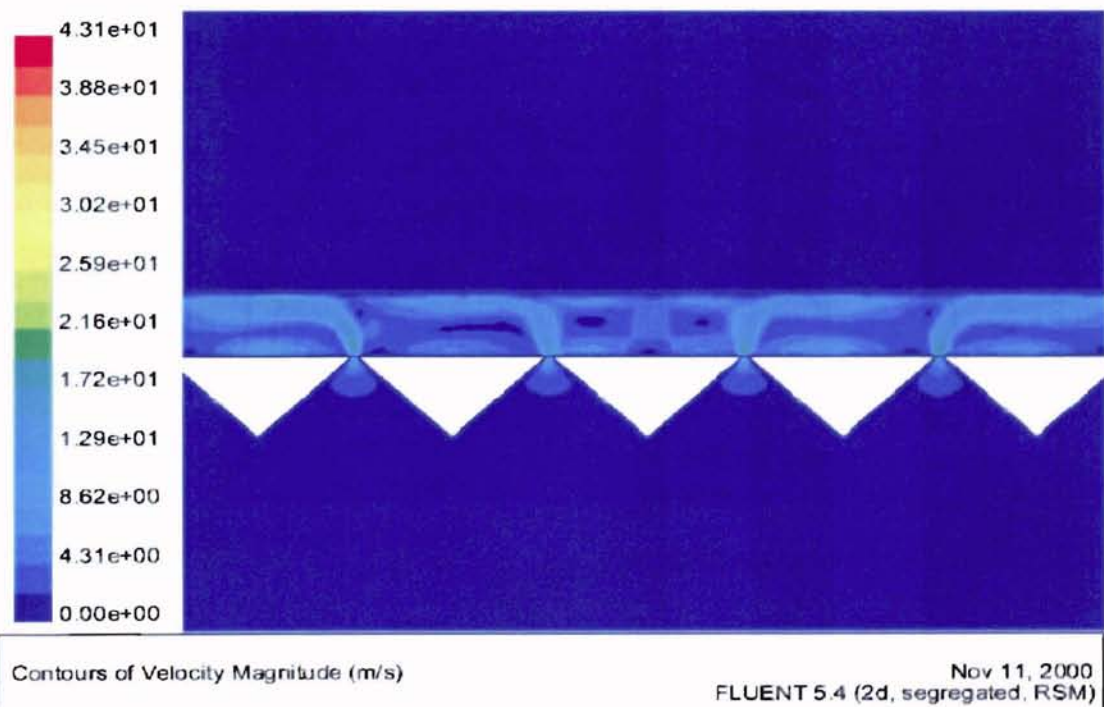
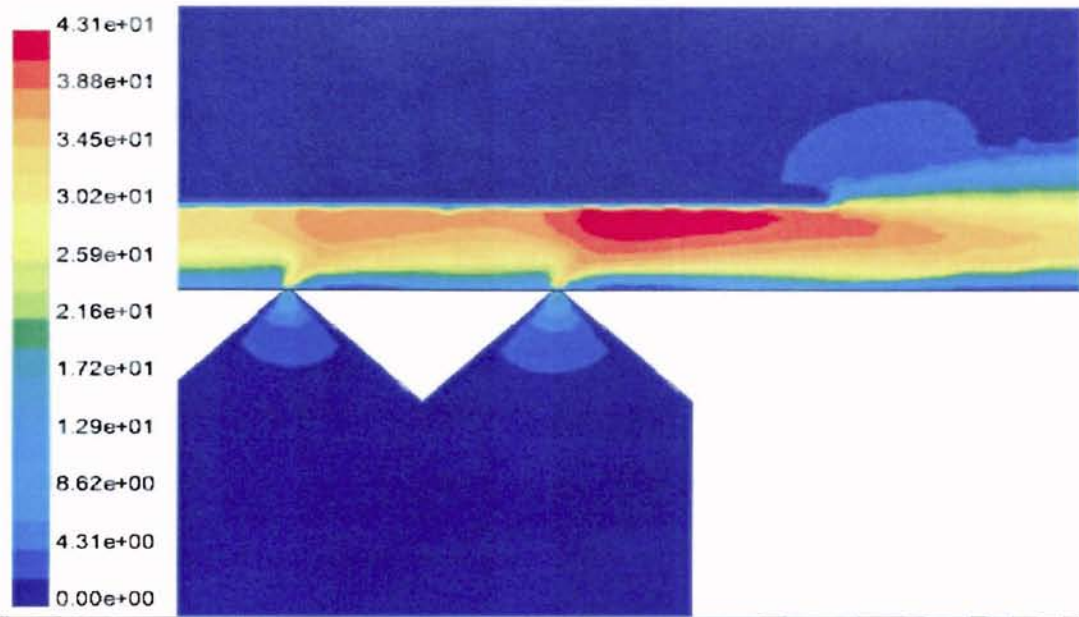


Figure 13. Velocity Contours in the Central Region ($h_c = 10$ mm and $\beta = 0$ deg)



Contours of Velocity Magnitude (m/s)

Nov 11, 2000
 FLUENT 5.4 (2d, segregated, RSM)

Figure 14. Velocity Contours near the Right Edge ($h_c = 10$ mm and $\beta = 0$ deg)

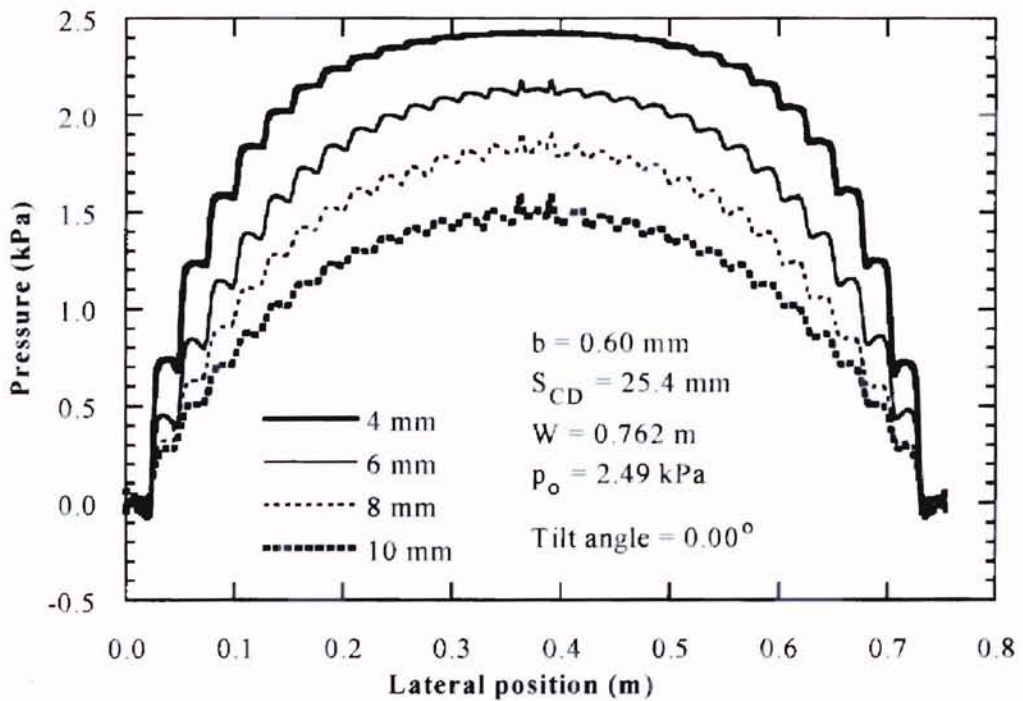


Figure 15. Effect of Flotation Height on Static Pressure Distribution on the Web

It is observed that the air velocity is very low in the central region (Figures 10 and 13), and it increases with the distance from the center. The flow velocity becomes maximum near the left and right edges of the web. The ripples in the pressure profile are due to the impingement of air jets. This effect is less significant near the central region for small flotation heights.

Static pressure reaches its maximum value in the central region and it decreases to the ambient pressure (zero gage pressure) at the edges. The static pressure tends to decrease with increase of flotation height. Figure 16 represents the effect of flotation height on shear stress on the web. The shape of the shear stress profiles on the web implies the net lateral force due to friction is zero. It is seen in Figure 16 that in the central region, the effect of jet impingement is more prominent for $h_c = 10$ mm than the $h_c = 4$ mm. The same trend is observed in Figure 15 also.

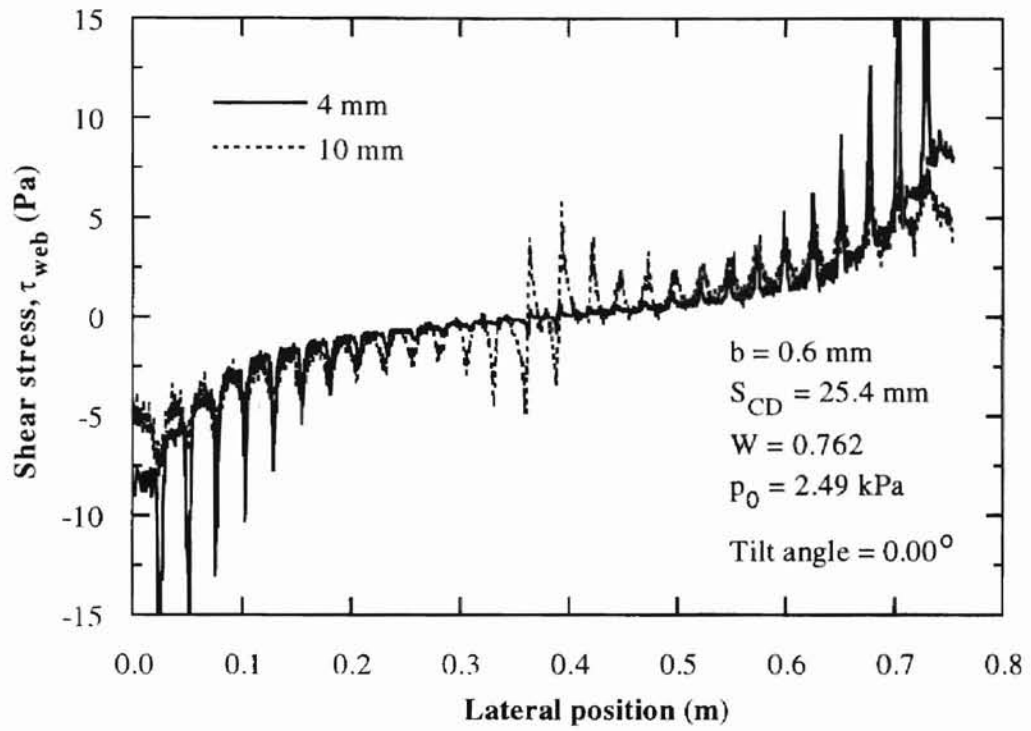


Figure 16. Effect of Flotation Height on Shear Stress

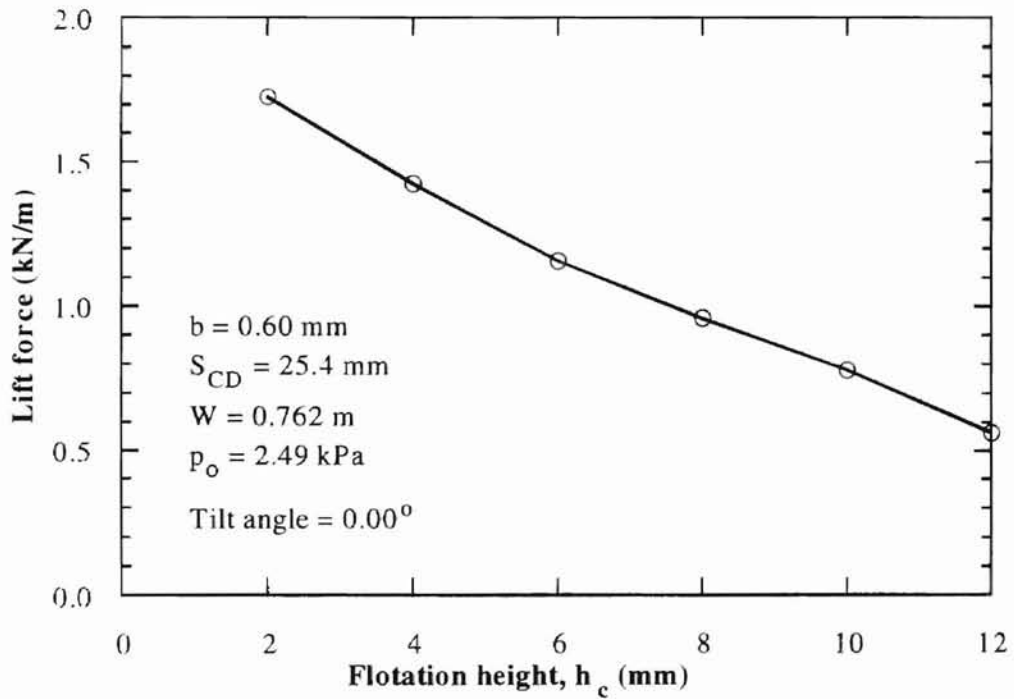


Figure 17. Effect of Flotation Height on Lift Force

4.2 Tilted Web

Aerodynamic forces on a tilted web are analyzed for various values of flotation height and tilt angle. The tilt angle is limited by the width of web and flotation height; one edge of web touches the air reverser when the tilt angle is large. Test conditions are listed in Table 1.

4.2.1 Static Pressure Distribution

Figures 18 through 21 represent static pressure profiles across the web for different flotation heights and different tilt angles.

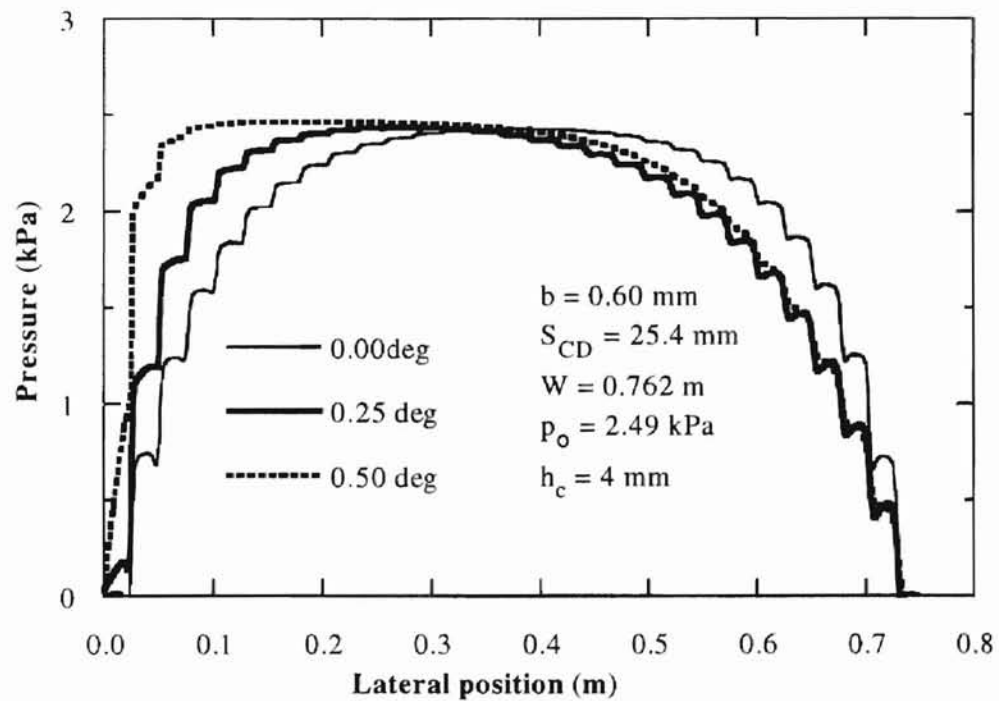


Figure 18. Effect of Tilt Angle on Pressure Distribution on the Web ($h_c = 4 \text{ mm}$)

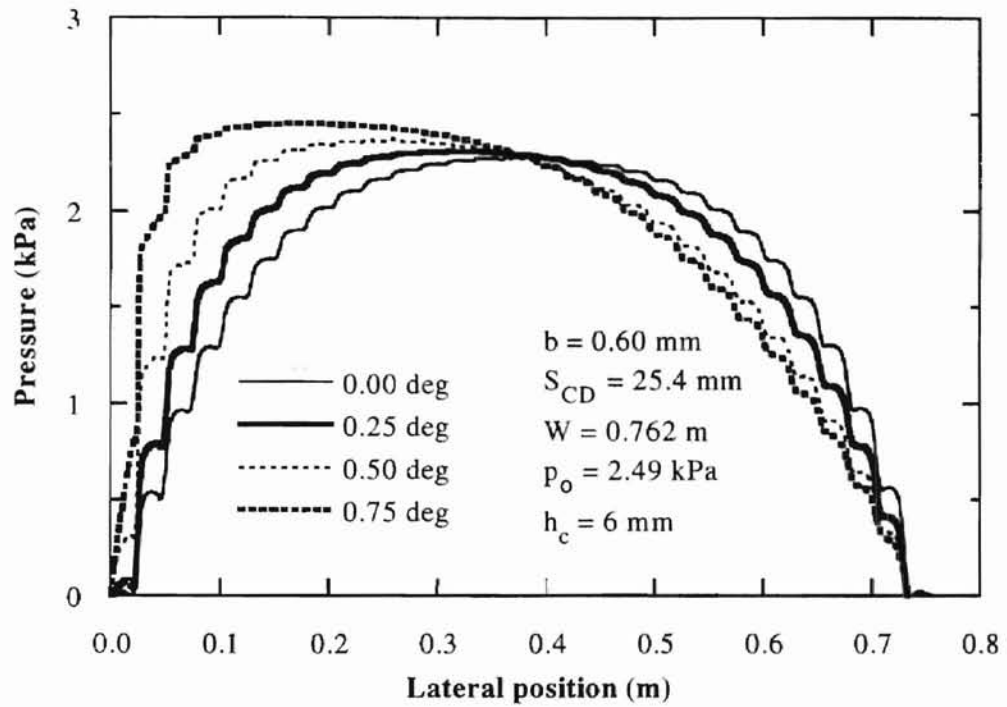


Figure 19. Effect of Tilt Angle on Pressure Distribution on the Web ($h_c = 6 \text{ mm}$)

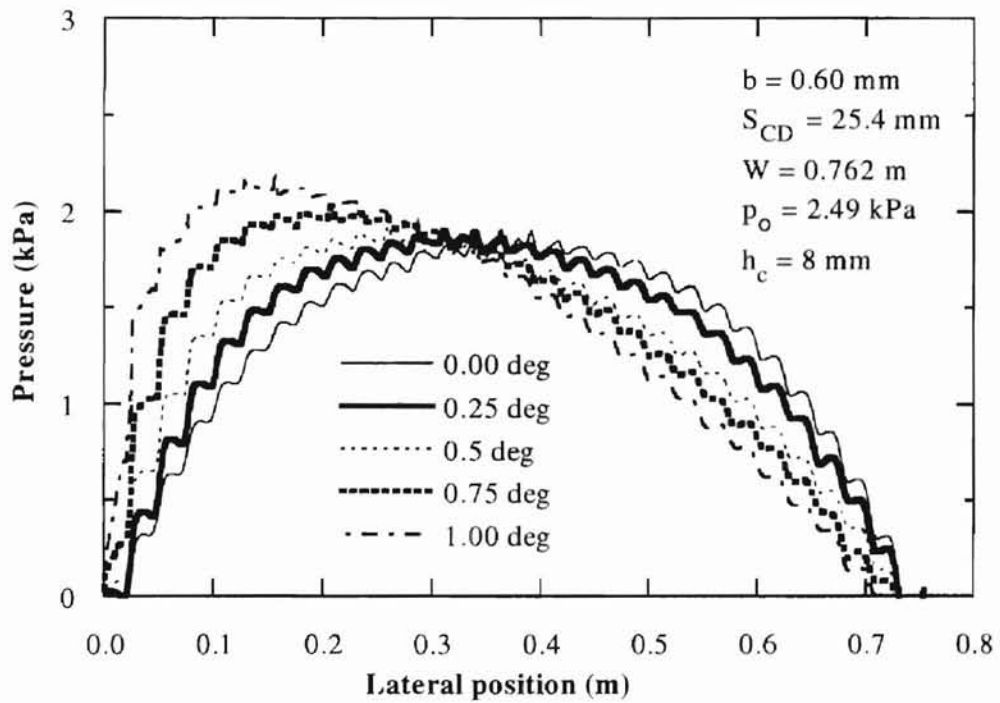


Figure 20. Effect of Tilt Angle on Pressure Distribution on the Web ($h_c = 8 \text{ mm}$)

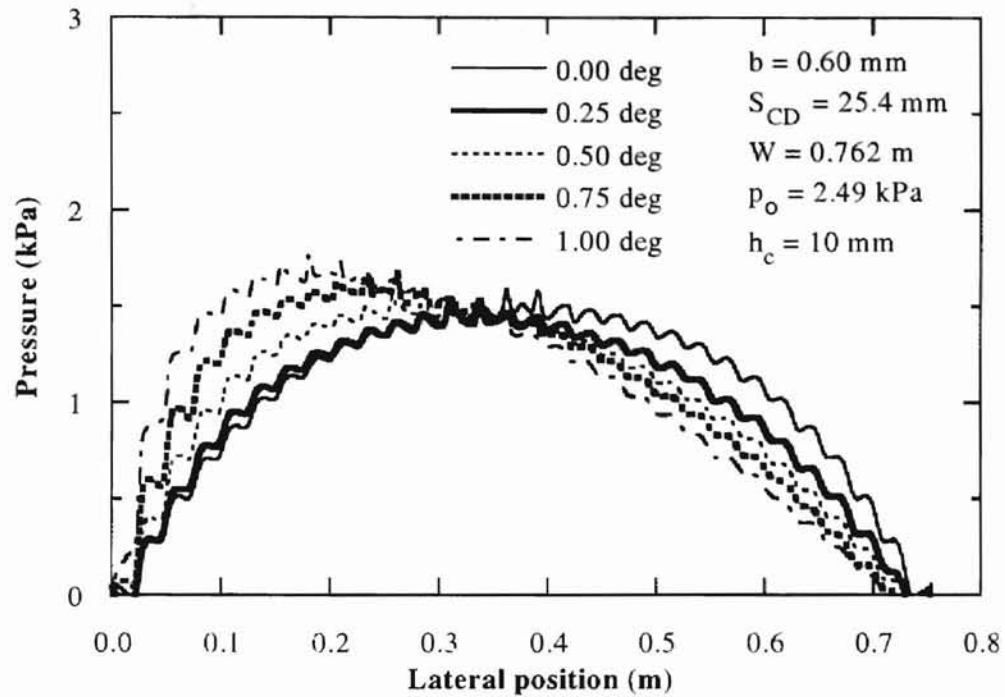


Figure 21. Effect of Tilt Angle on Pressure Distribution on the Web ($h_c = 10$ mm)

It is seen, in Figures 18 through 21, that the pressure profile becomes asymmetric when the web is tilted. The location where the cushion pressure is maximum moves towards the left edge (the closer to the air reverser surface than the other edge). Note that the location of maximum pressure is the transition point where the direction of air flow changes. For example if we consider the case of $h_c = 10$ mm and $\beta = 1.00$ degree shown in Figure 21, the air in the region $0 \leq x < 0.17$ m flows toward the left hand side edge, while the air in the region $0.17 \leq x < 0.762$ m moves in the opposite direction. Note also that the effect of the horizontal flow on the jet flow is more significant near the right hand side edge, where the flotation height is larger than the other edge.

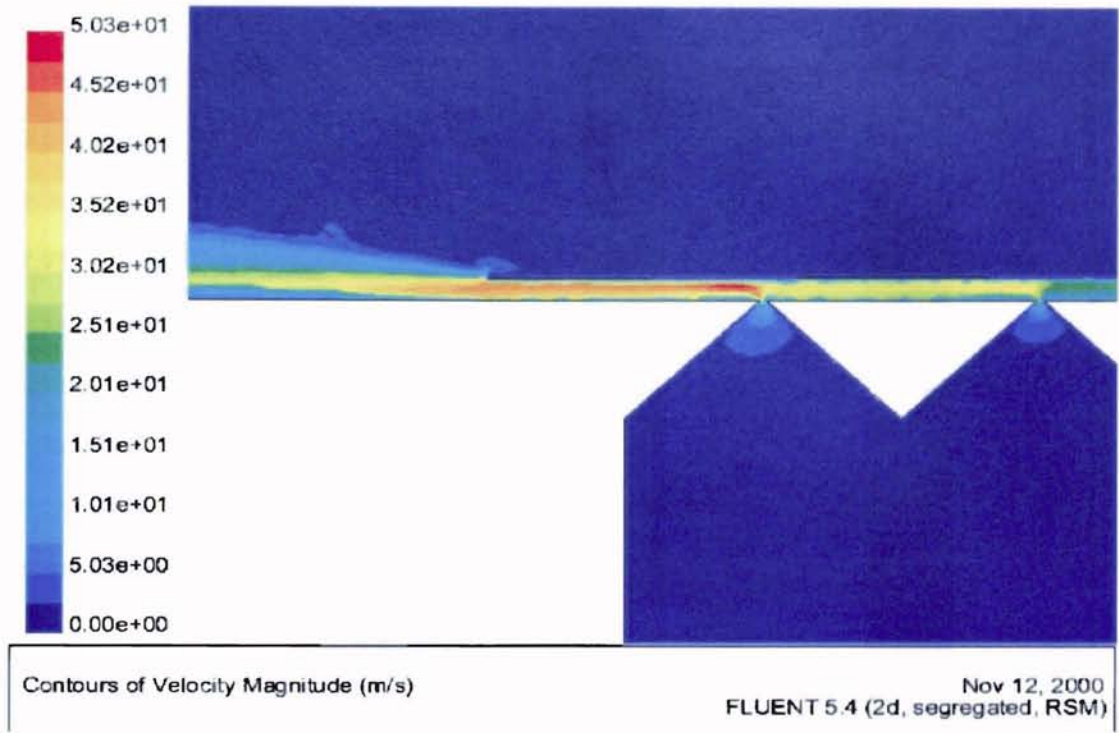


Figure 22. Velocity Contours near the Left Edge ($h_c = 4 \text{ mm}$ and $\beta = 0.50 \text{ deg}$)

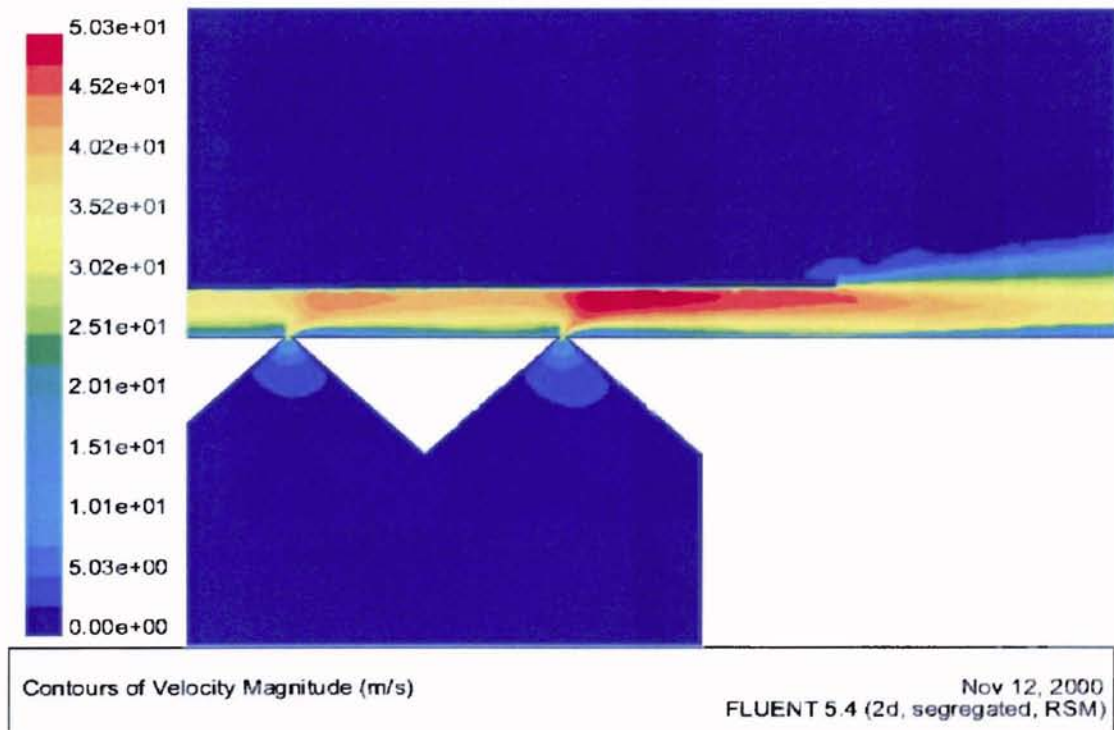
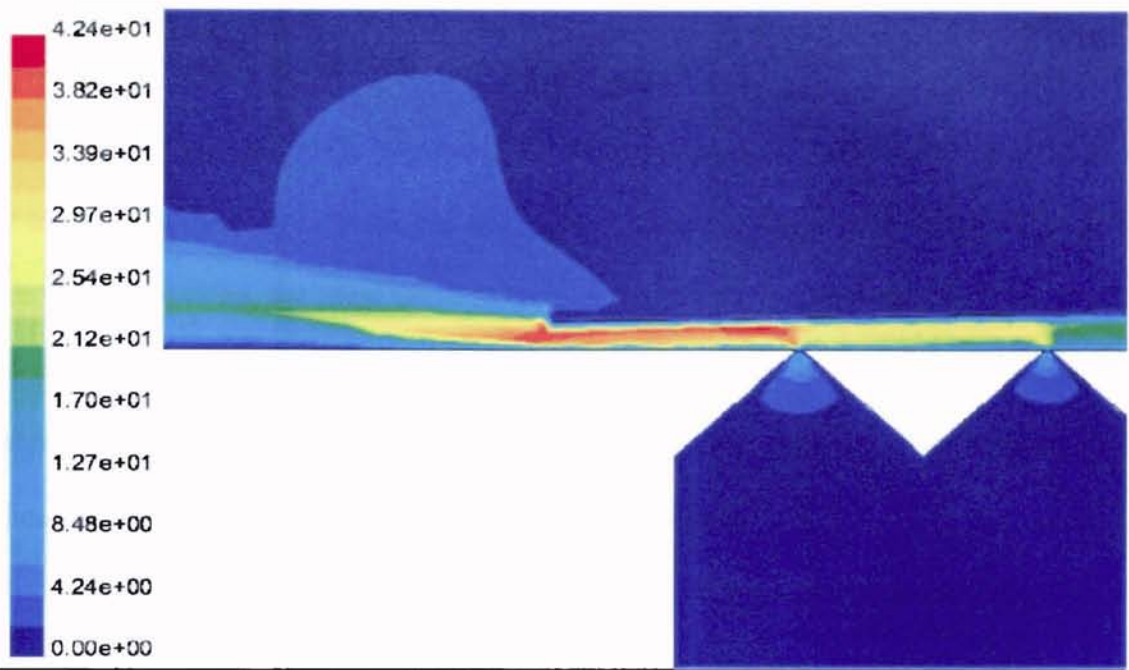


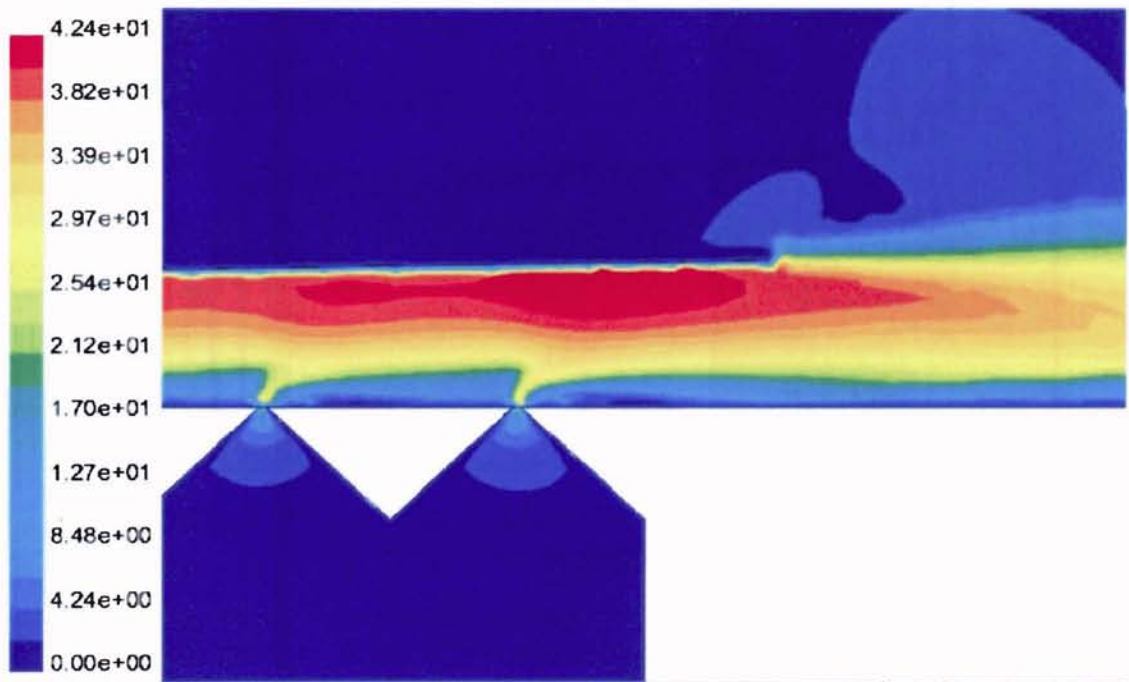
Figure 23. Velocity Contours near the Right Edge ($h_c = 4 \text{ mm}$ and $\beta = 0.50 \text{ deg}$)



Contours of Velocity Magnitude (m/s)

Nov 12, 2000
 FLUENT 5.4 (2d, segregated, RSM)

Figure 24. Velocity Contours near the Left Edge ($h_c = 10$ mm and $\beta = 1.00$ deg)



Contours of Velocity Magnitude (m/s)

Nov 12, 2000
 FLUENT 5.4 (2d, segregated, RSM)

Figure 25. Velocity Contours near the Right Edge ($h_c = 10$ mm and $\beta = 1.00$ deg)

4.2.2 Shear Stress Distribution

Wall shear stress (aerodynamic friction) profiles are obtained for various values of the average floatation height and tilt angle as shown in Figures 26 through 29. When the web is not tilted, the shear stress magnitudes appear to be symmetric but the direction of stress changes in the central region where the direction of flow changes. The net lateral force, therefore, is to be zero as discussed in later section. The sharp spikes in shear stress graphs are due to the impingement effect of air jets.

When the web is tilted, the shear stress magnitude profile loses symmetry and the location where the shear stress changes its direction moves towards the left edge.

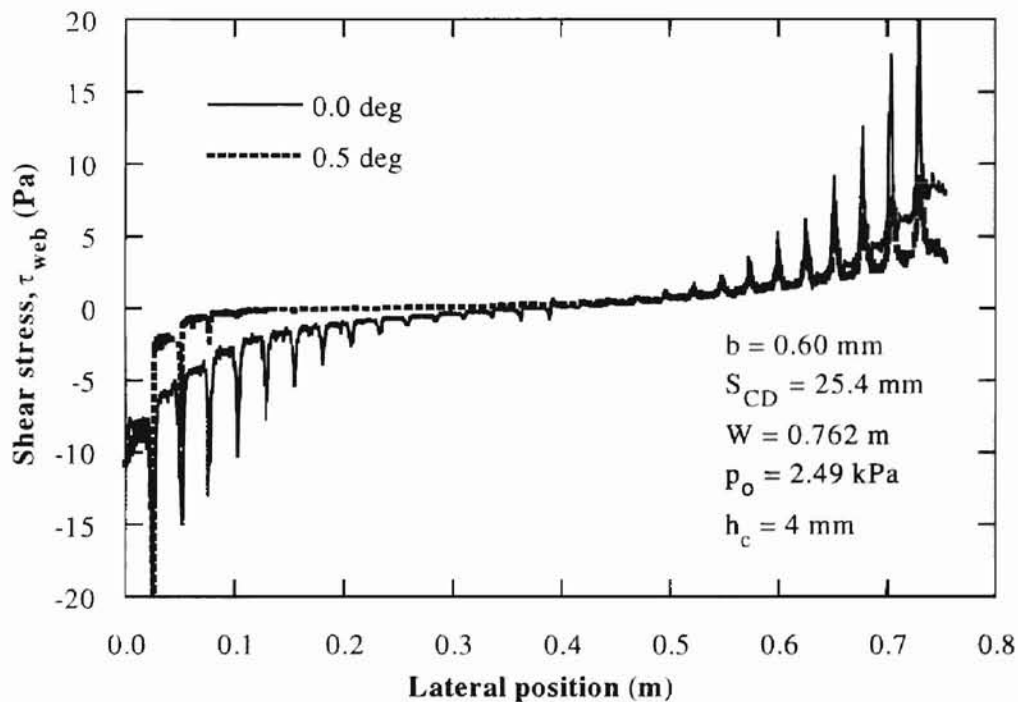


Figure 26. Effect of Tilt Angle on Shear Stress ($h_c = 4 \text{ mm}$)

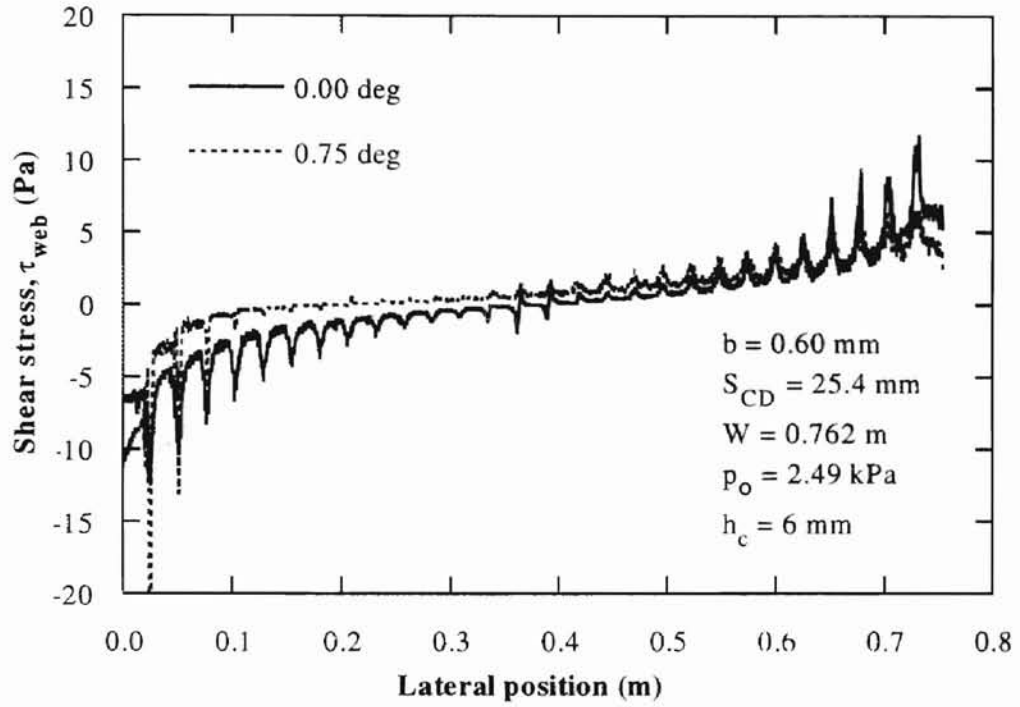


Figure 27. Effect of Tilt Angle on Shear Stress ($h_c = 6$ mm)

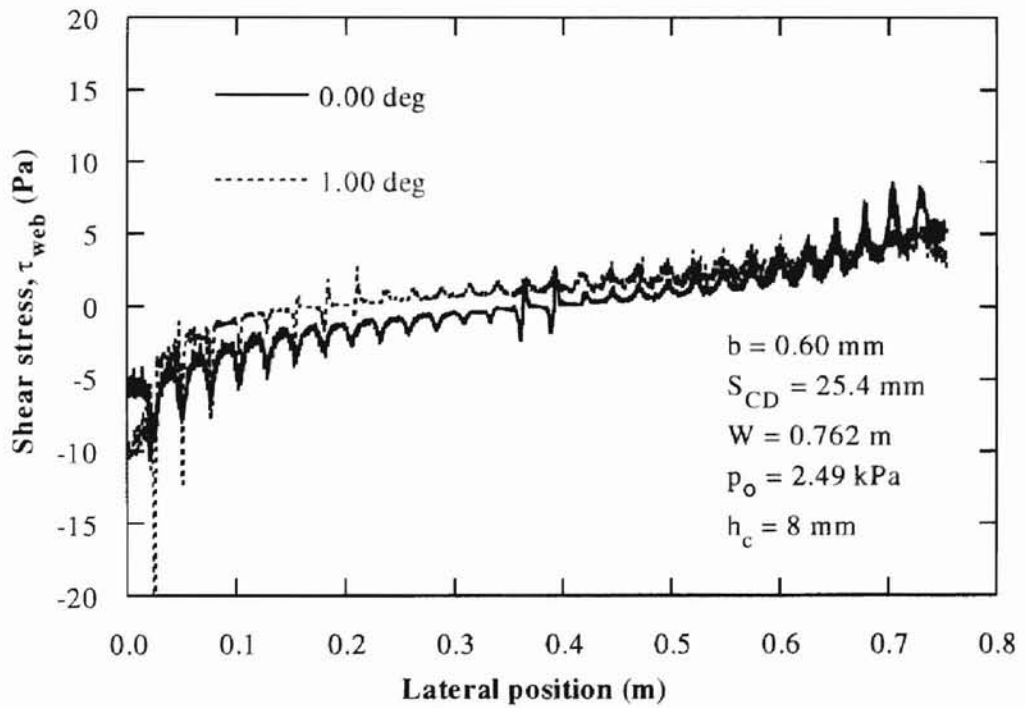


Figure 28. Effect of Tilt Angle on Shear Stress ($h_c = 8$ mm)

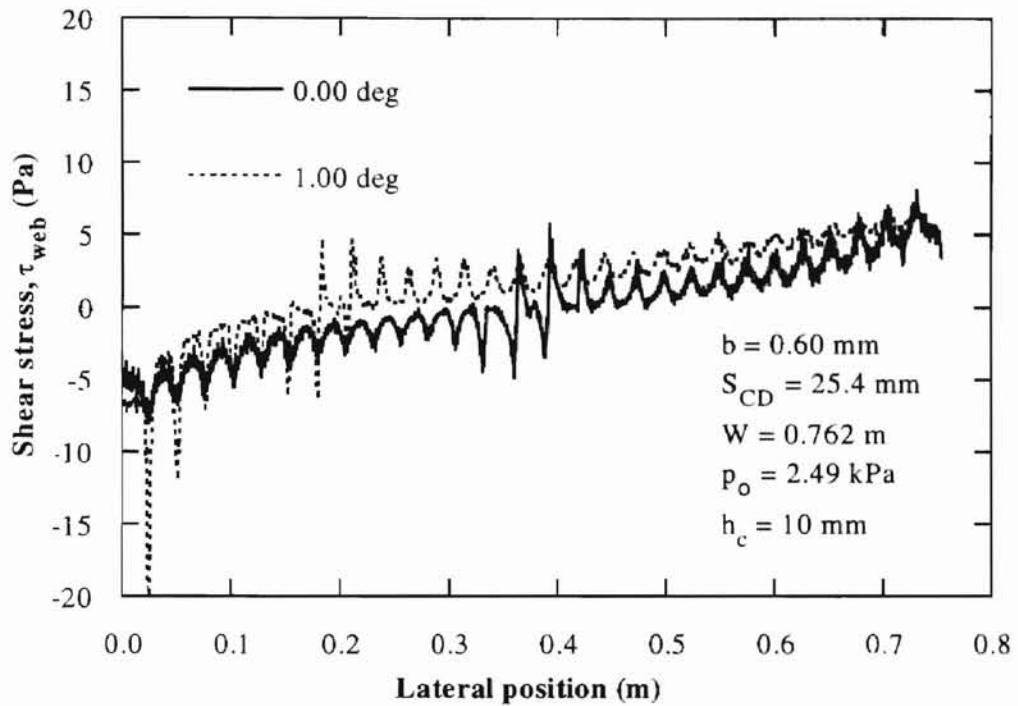


Figure 29. Effect of Tilt Angle on Shear Stress ($h_c = 10$ mm)

4.2.3 Lift Force

Lift force per unit length of the web is obtained by integrating the pressure profile along the width of the web.

$$L = \int_0^w p \cdot dy \quad (3)$$

The trapezoidal method is used for approximating the lift force on the web. The graph is re-plotted in Figure 31 to show the lift force data normalized by the values for non-tilted web. It is seen that the effect of tilt angle on the lift force is insignificant in the range of computations.

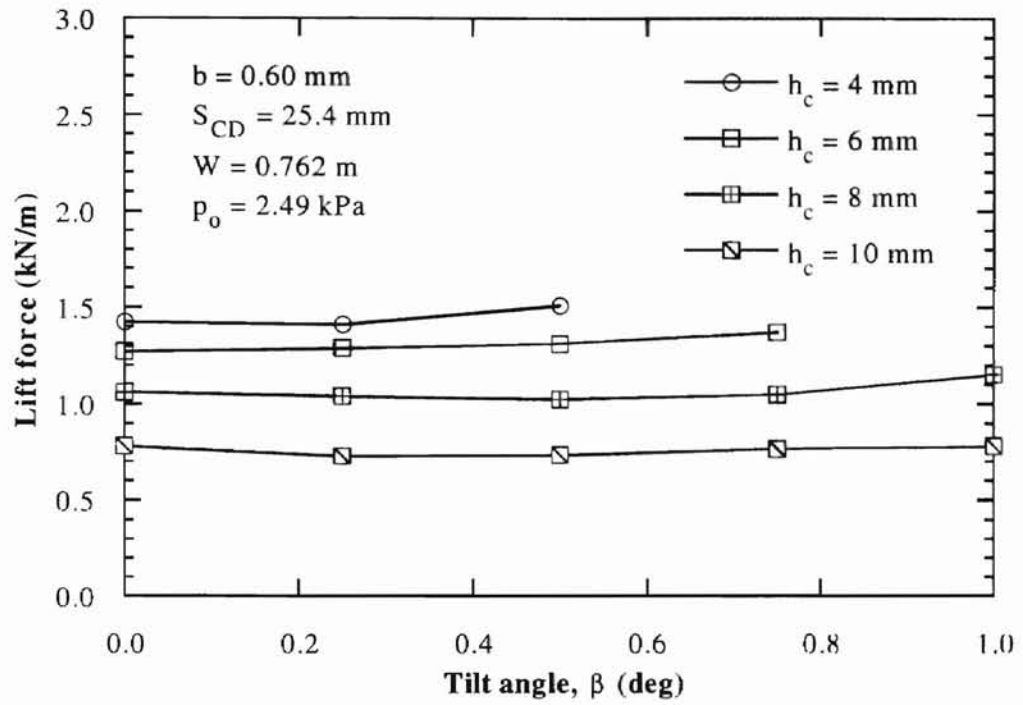


Figure 30. Effect of Tilt Angle on Lift Force

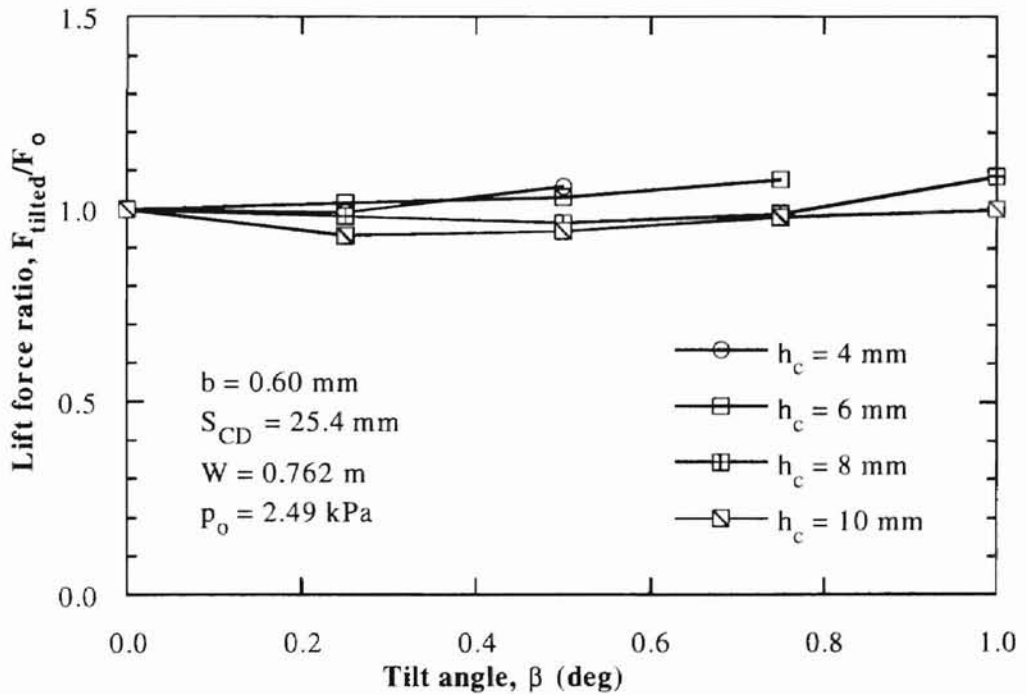


Figure 31. Effect of Tilt Angle on Lift Force Ratio

4.2.4 Lateral Forces

Lateral aerodynamic force on a tilted web is from two causes: aerodynamic pressure and friction. The lateral force due to aerodynamic pressure is obtained by multiplying the lift force with the sine of tilt angle. That is,

$$\begin{aligned} F_{y(\text{due to pressure})} &= -F_y \sin(\beta) \\ &= -\int_0^w p dy \sin(\beta) \end{aligned} \quad (4)$$

The lateral force due to friction is obtained by integrating the wall shear stress profile along the width of the web.

$$F_{y(\text{due to friction})} = \int_0^w \tau_{web} \cdot dy \quad (5)$$

These two effects (pressure and friction) are compared in Figure 32 for the average floatation height of 4 mm for various values of tilt angle. It is clear that the effect of pressure loading is dominant, and the effect of aerodynamic friction is practically negligible. The same trend is observed for all different values of the average floatation height considered (Figures 33 through 35).

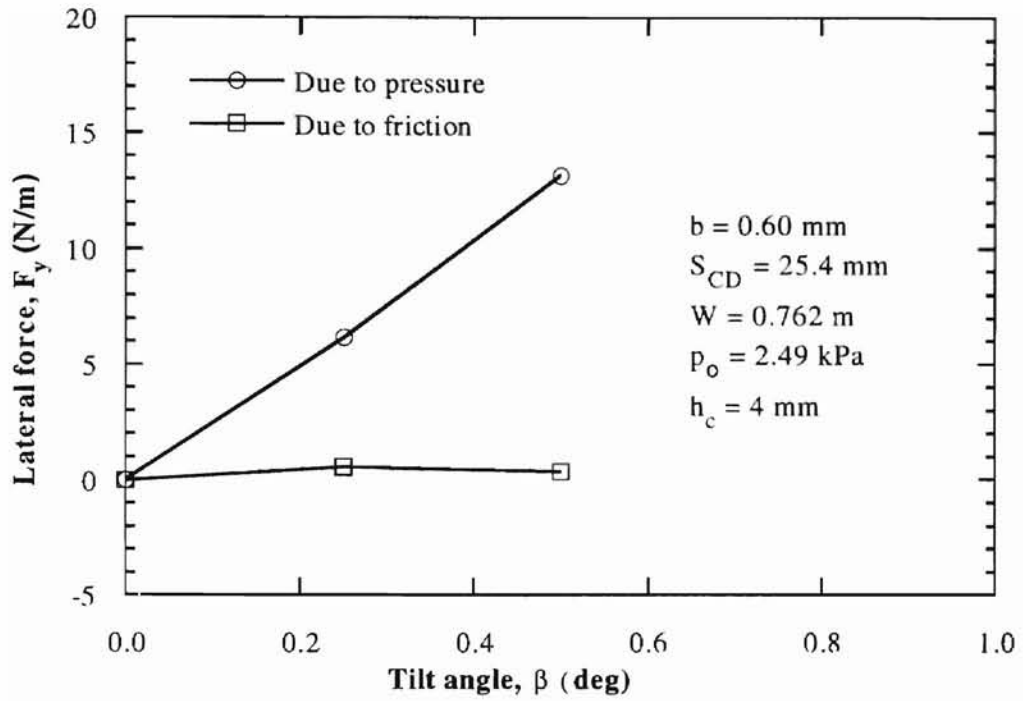


Figure 32. Effect of Tilt Angle on the Lateral Force ($h_c = 4$ mm)

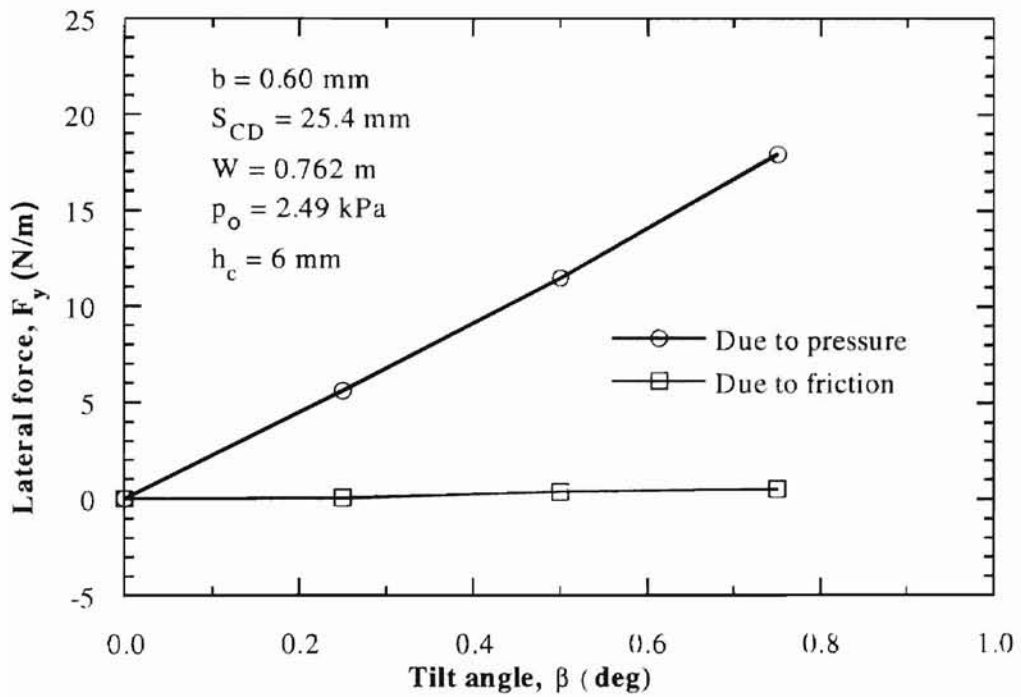


Figure 33. Effect of Tilt Angle on the Lateral Force ($h_c = 6$ mm)

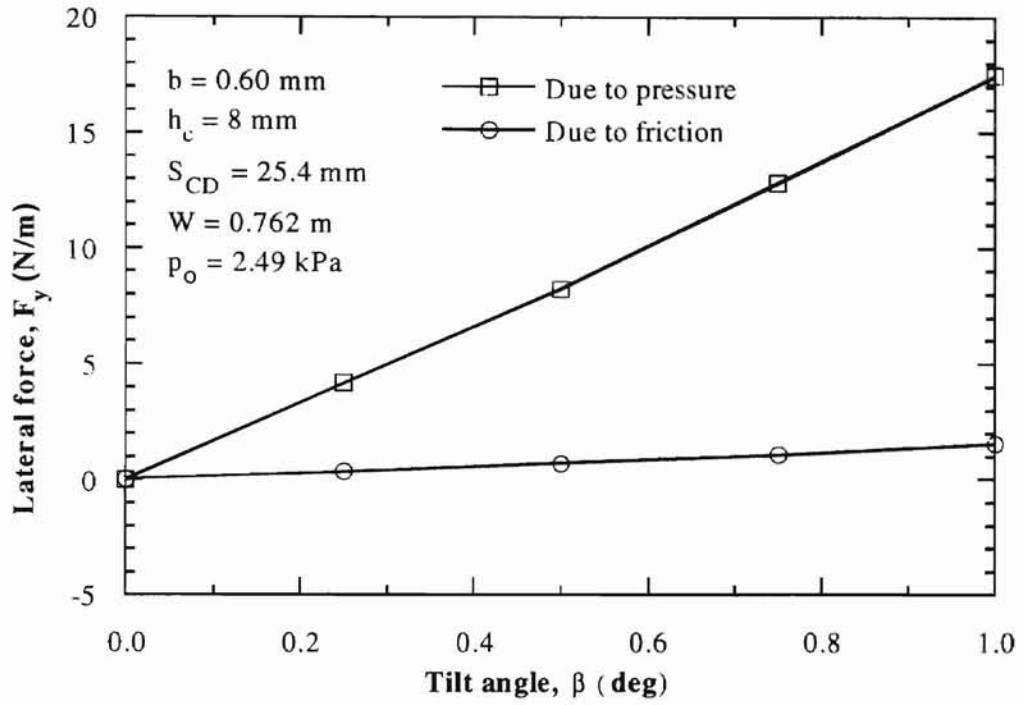


Figure 34. Effect of Tilt Angle on the Lateral Force ($h_c = 8 \text{ mm}$)

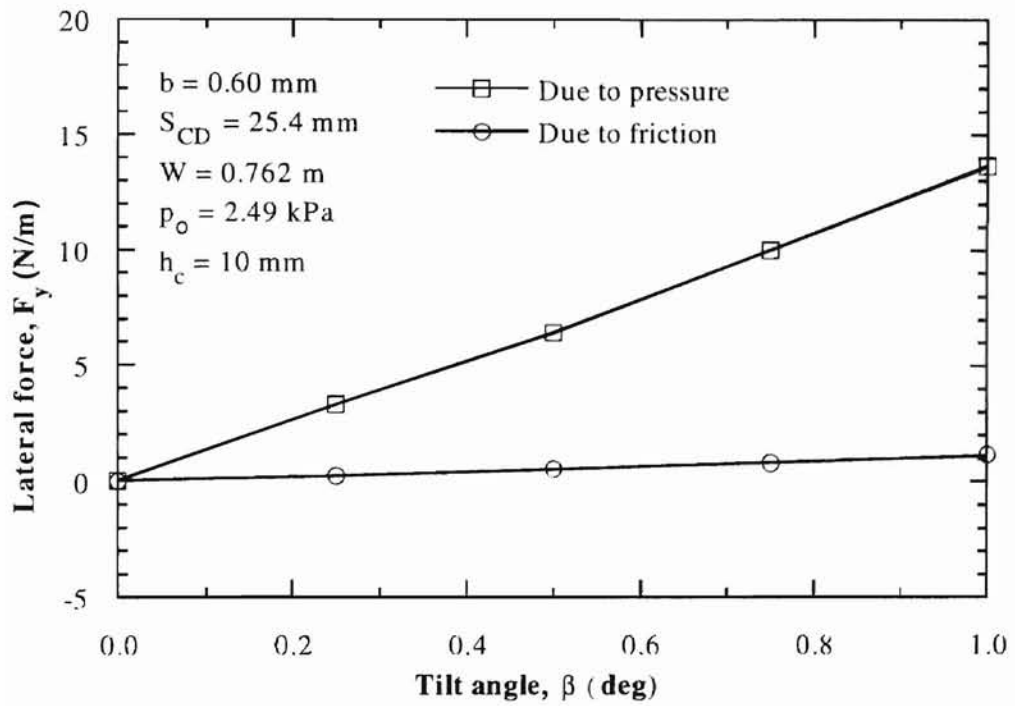


Figure 35. Effect of Tilt Angle on the Lateral Force ($h_c = 10 \text{ mm}$)

The lateral force due to pressure loading is shown in Figure 36 as a function of tilt angle for different values of average flotation height. It clearly shows that the lateral force increases with the tilt angle but decreases when the flotation height increases. The range of tilt angle is limited in the graph because the web touches the air reverser surface when the angle is too large.

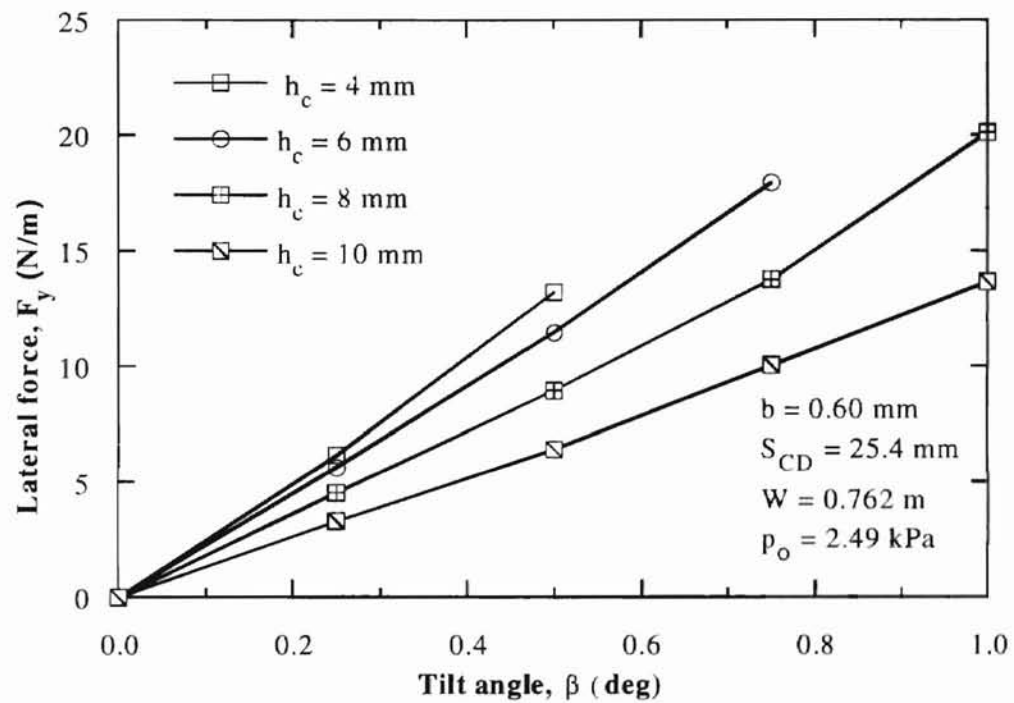


Figure 36. Lateral Aerodynamic Force on Tilted Web

4.2.4 Discharge Coefficient

The affect of discharge coefficient is discussed in this section. The mass flow rate of a round jet can be calculated as

$$Q_{hole} = C\rho \frac{\pi d^2}{4} \sqrt{\frac{2\Delta p}{\rho}} \quad (6)$$

and the mass flow rate of a plane jet per unit length through the slot of width b can be calculated as

$$Q_{slot} = C\rho b\sqrt{\frac{2\Delta p}{\rho}} \quad (7)$$

where C is the coefficient of discharge, which is known as 0.6 (Roberson and Crow, 1978). Discharge coefficient is calculated based on the computational results. FLUENT can directly provide the mass flow rate of a jet through a slot. The average pressure in the web-reverser clearance is calculated by creating two points on the surface using “Point” command and then calculating pressure at each point. Table 2 represents the mass flow rate, pressure in the gap, pressure difference, and discharge coefficient for each flotation height considered. In the table, the “pressure in the gap” means the average value of two gage pressures determined on the air reverser surface at ± 12.7 mm (0.5 inches) from the center of the slot nozzle, and “pressure difference” indicates the difference between the supply pressure ($p_o = 2.49$ kPa) and the pressure in the gap. As seen in Figure 37, the discharge coefficient varies with the flotation height.

Table 2. Values of Variables Used to Determine Discharge Coefficient

h_c (mm)	Mass Flow Rate (kg/ms)	Pressure in the Gap (kPa)	Pressure Difference (kPa)	Discharge Coefficient
4	0.00643	2.417	0.073	0.801
6	0.01338	2.204	0.286	0.840
8	0.01948	1.931	0.559	0.875
10	0.02421	1.549	0.941	0.839
12	0.02703	1.209	1.281	0.802

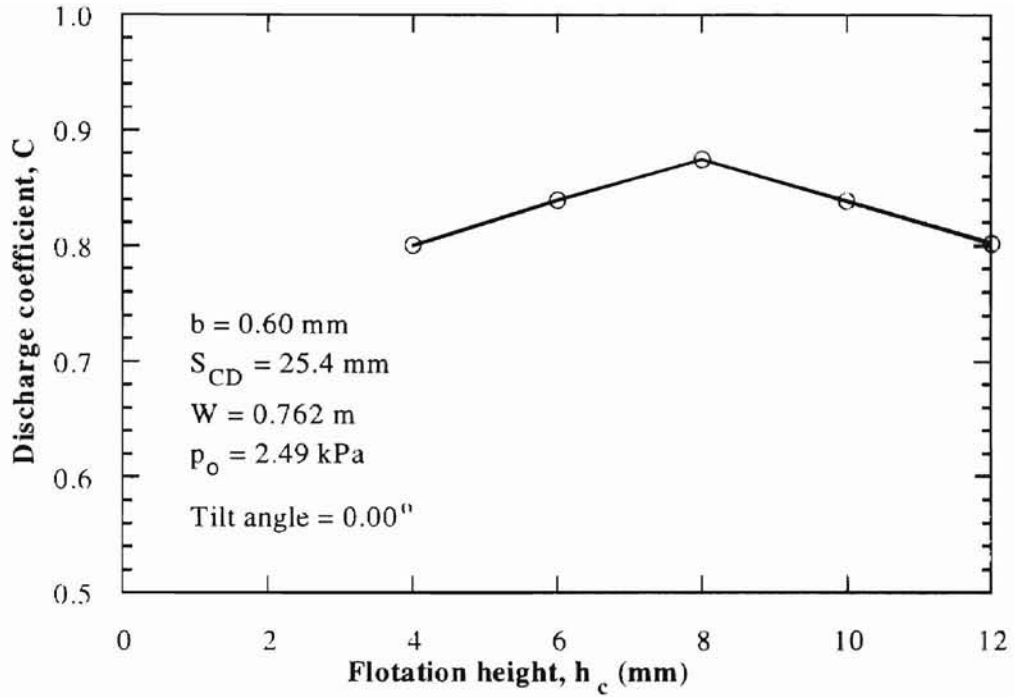


Figure 37. Variation of Discharge Coefficient

4.3 Comparison with Analytical Results

The CFD (Computational Fluid Dynamics) results are compared with the analytical model developed by Chang (October 2000). The analytical pressure profile on the web is

$$p_{web} = p_o - p_o \left(1 - \frac{2Cb}{S_{CD}} \right) \left[\frac{e^{-\alpha y} + e^{-\alpha W} e^{\alpha y}}{1 + e^{-\alpha W}} \right]^2 \quad (8)$$

and the analytical lift force per unit length of web is

$$L = p_o W - p_o \left(1 - \frac{2Cb}{S_{CD}} \right) \left[\frac{1 - e^{-2\alpha W} + 2\alpha e^{-\alpha W} W}{\alpha(1 + e^{-\alpha W})^2} \right]^2 \quad (9)$$

where $\alpha = \sqrt{2} \frac{Cb}{HS_{CD}}$, and H is the flotation height which is constant.

4.3.1 Pressure Distribution

The computed pressure profiles obtained using FLUENT are compared with the analytical model (Chang, October 2000). In all cases considered, as shown in Figures 38 to 41, the analytical model under predicts the cushion pressure when compared with the computational results. Note that the discharge coefficient is assumed 0.60 in the analytical model, while current computational study shows that the discharge coefficient varies with the flotation height (Figure 37).

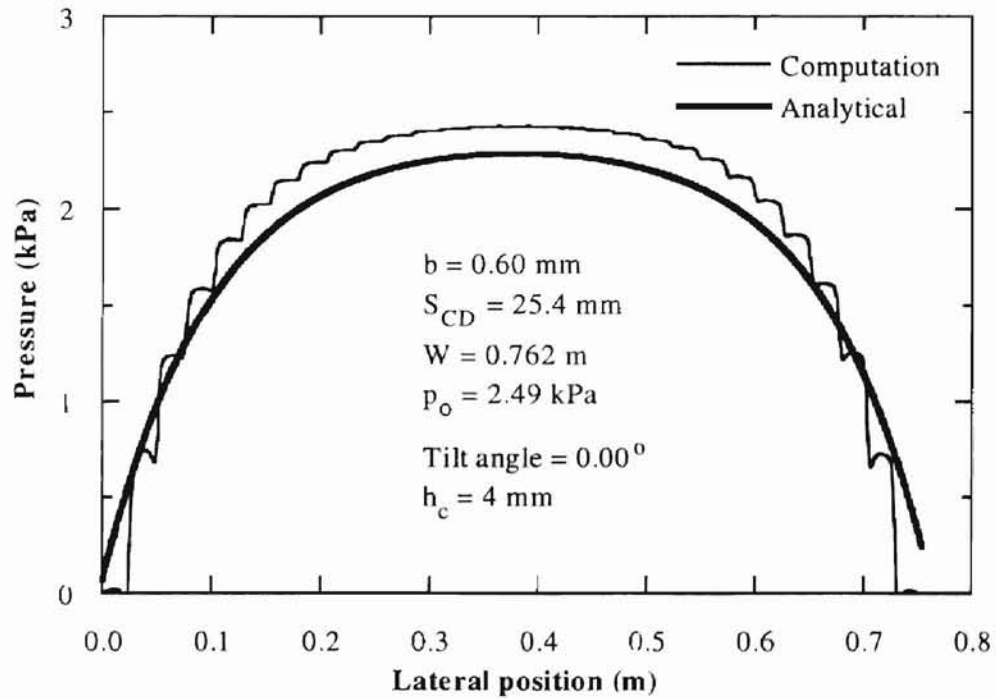


Figure 38. Comparison of Pressure Profiles for $h_c = 4 \text{ mm}$

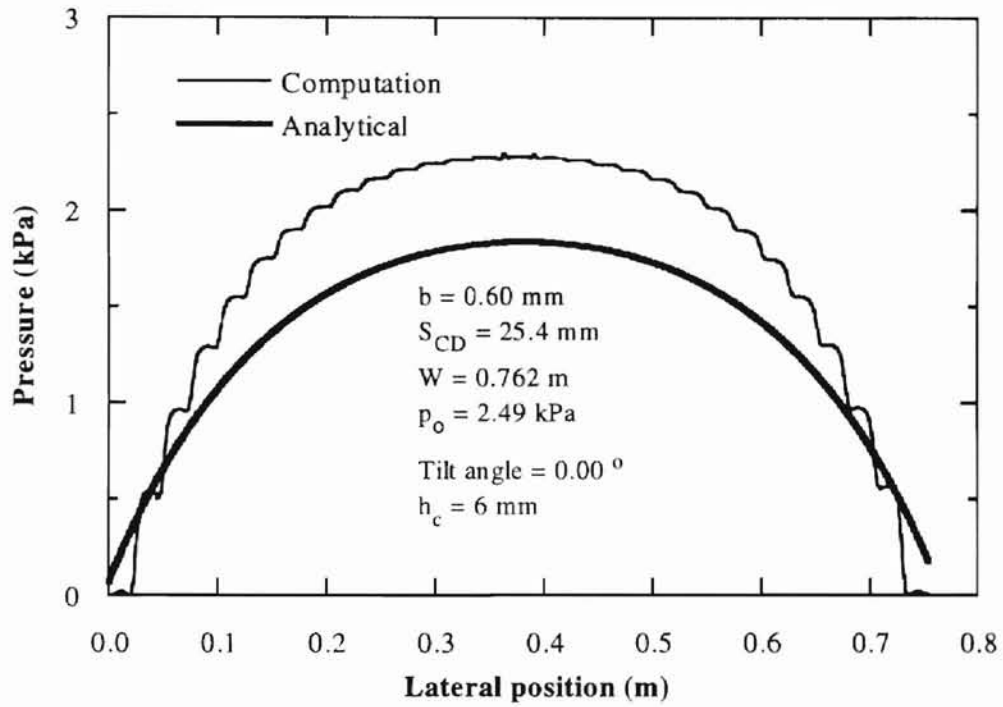


Figure 39. Comparison of Pressure Profiles for $h_c = 6 \text{ mm}$

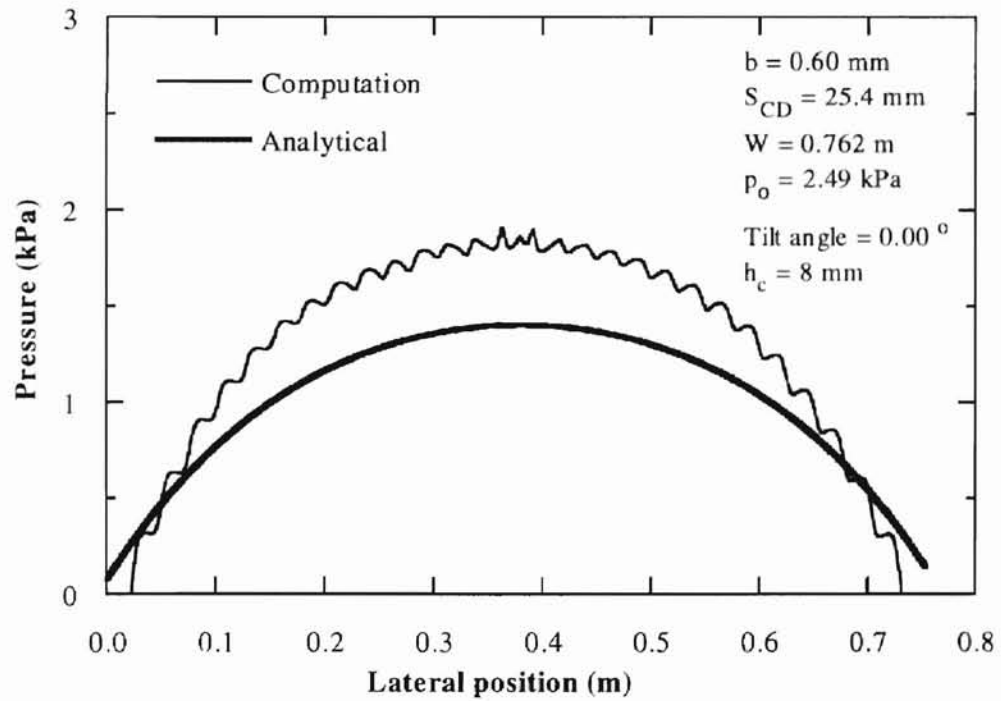


Figure 40. Comparison of Pressure Profiles for $h_c = 8 \text{ mm}$

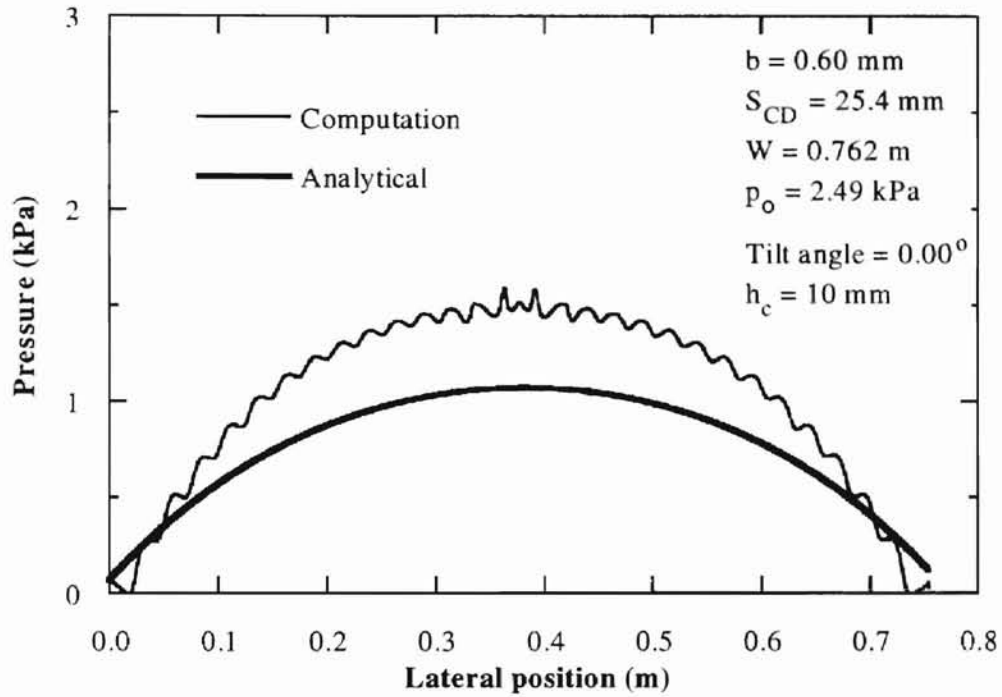


Figure 41. Comparison of Pressure Profiles for $h_c = 10$ mm

4.3.2 Lift Force and Lateral Force

The computational lift force tends to overpredict when compared with Chang's analytical model, and the difference increases with the flotation height, as shown in Figure 42. Figure 43 through 46 show comparisons of lateral force. Note that the analytical model determines the lift force for only non-tilted web so that the analytical lateral force is

$$F_y = F_{non-tilted} \sin(\beta) \quad (10)$$

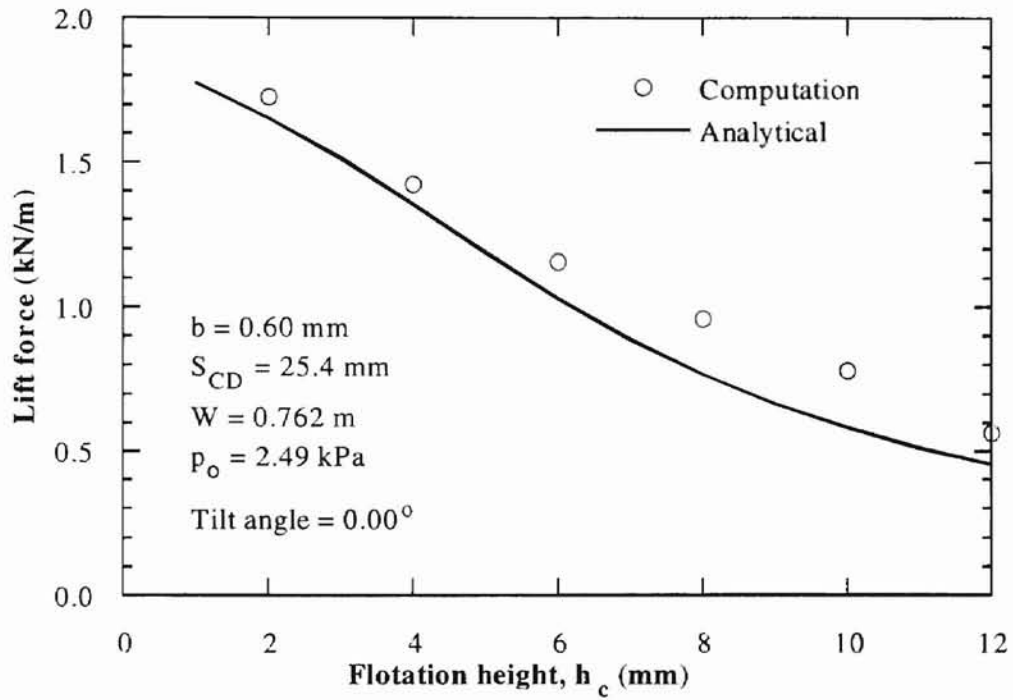


Figure 42. Comparison of Lift Forces for $\beta = 0.00$ deg

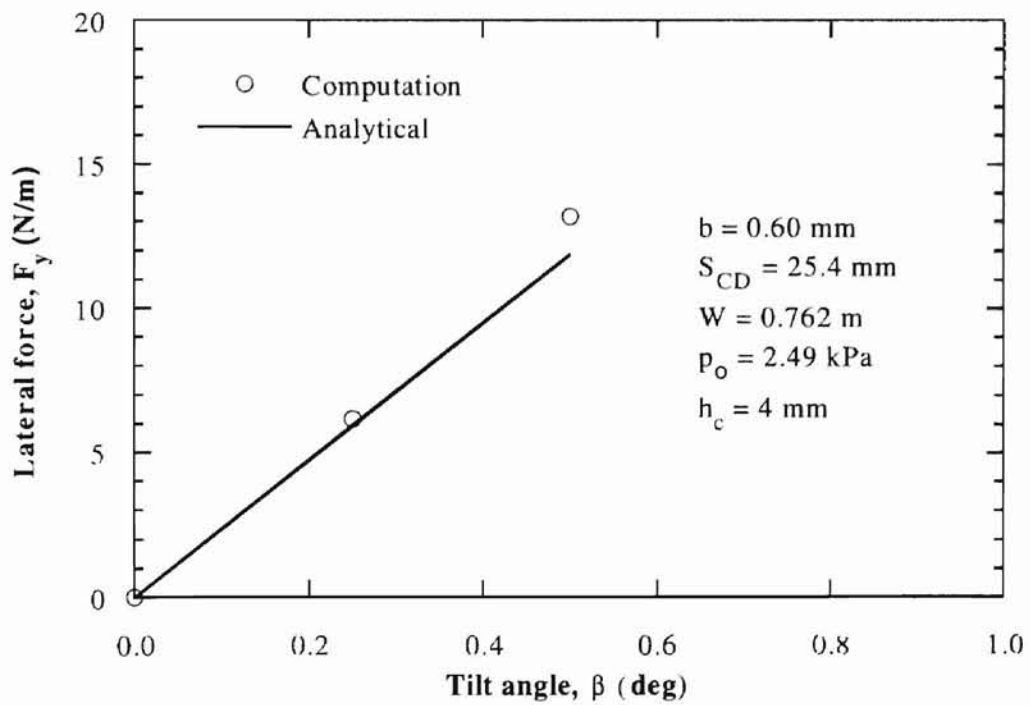


Figure 43. Comparison of Lateral Forces for $h_c = 4$ mm

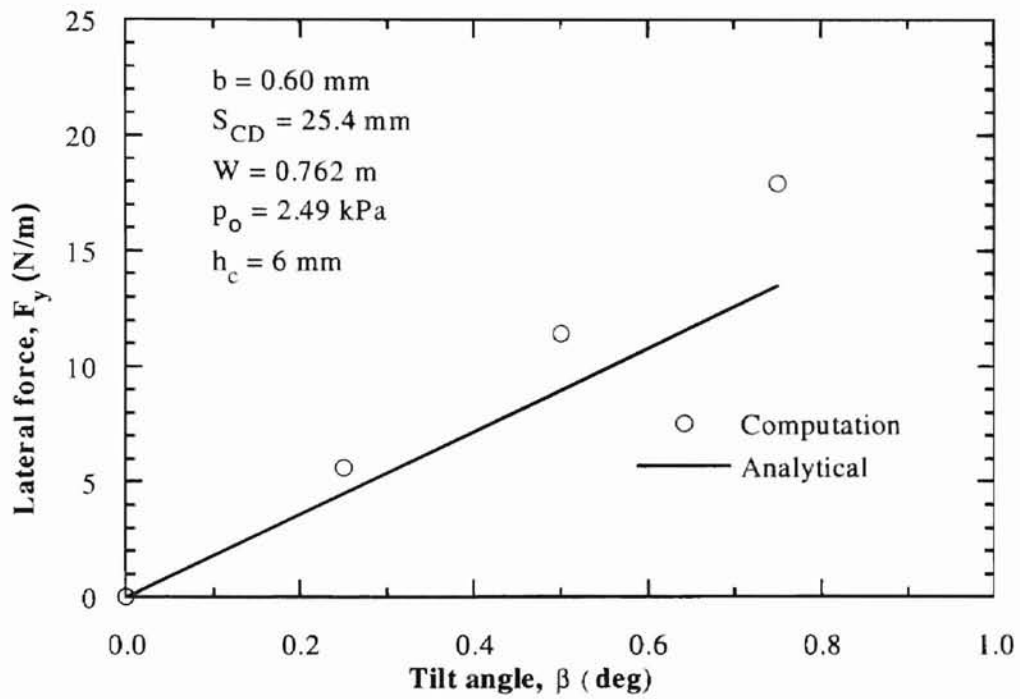


Figure 44. Comparison of Lateral Forces for $h_c = 6 \text{ mm}$

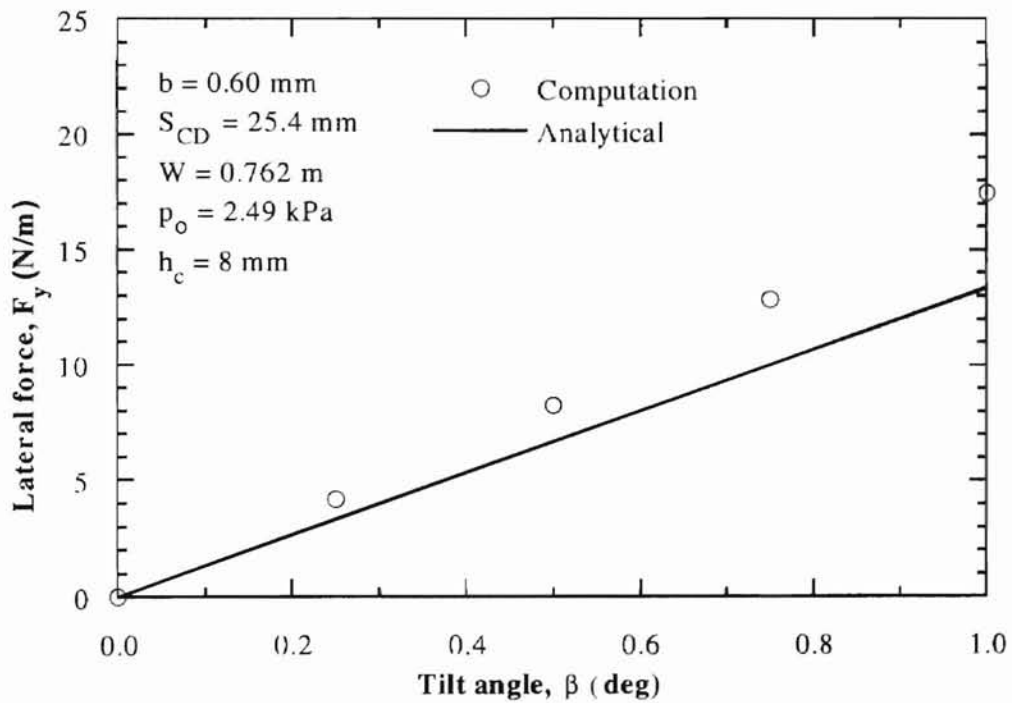


Figure 45. Comparison of Lateral Forces for $h_c = 8 \text{ mm}$

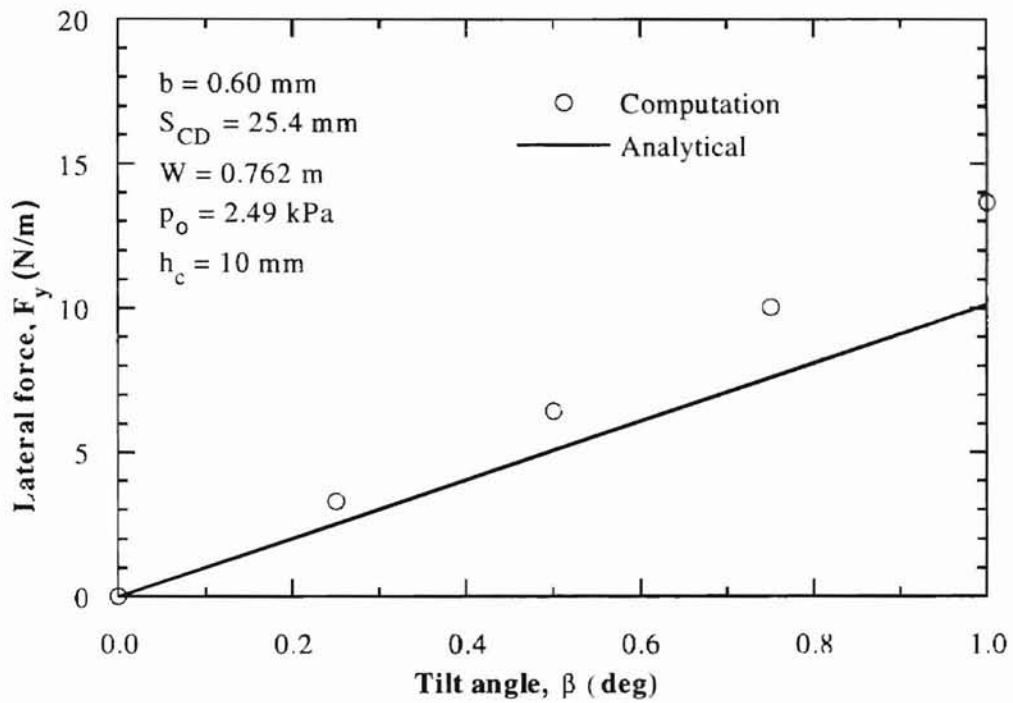


Figure 46. Comparison of Lateral Forces for $h_c = 10 \text{ mm}$

The computational pressure profiles are compared again with Chang's analytical model but with a modification to the discharged coefficient for the analytical model. The discharge coefficient is corrected based on the computed values, the computational and analytical pressure profile seem to agree well as shown in Figures 47 through 50.

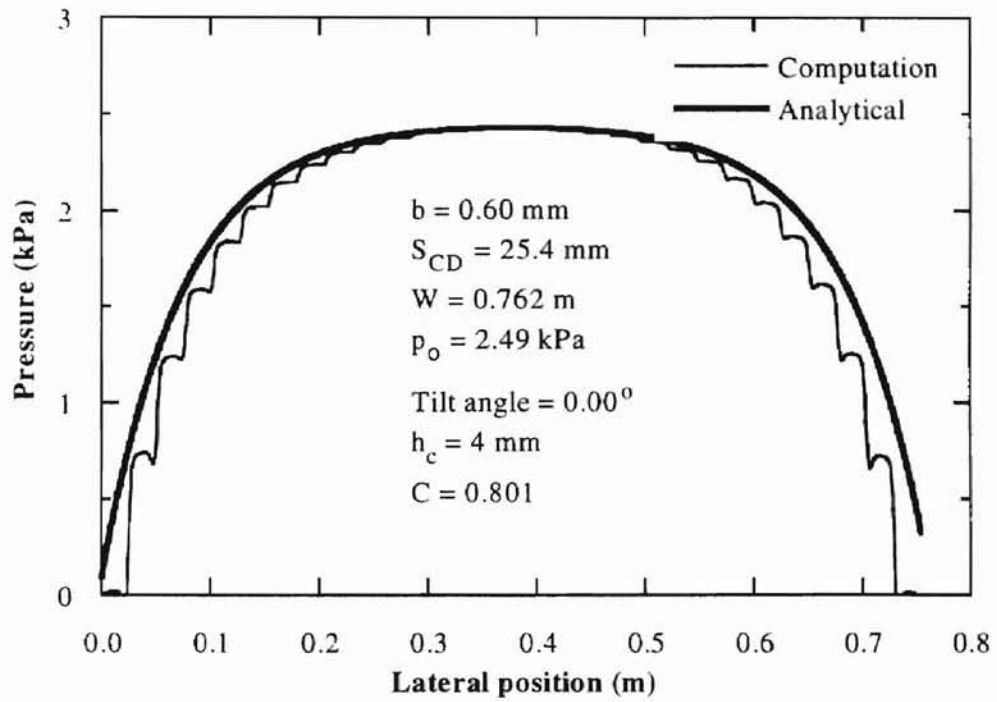


Figure 47. Comparison of Pressure Profiles for $h_c = 4 \text{ mm}$ and $C = 0.801$

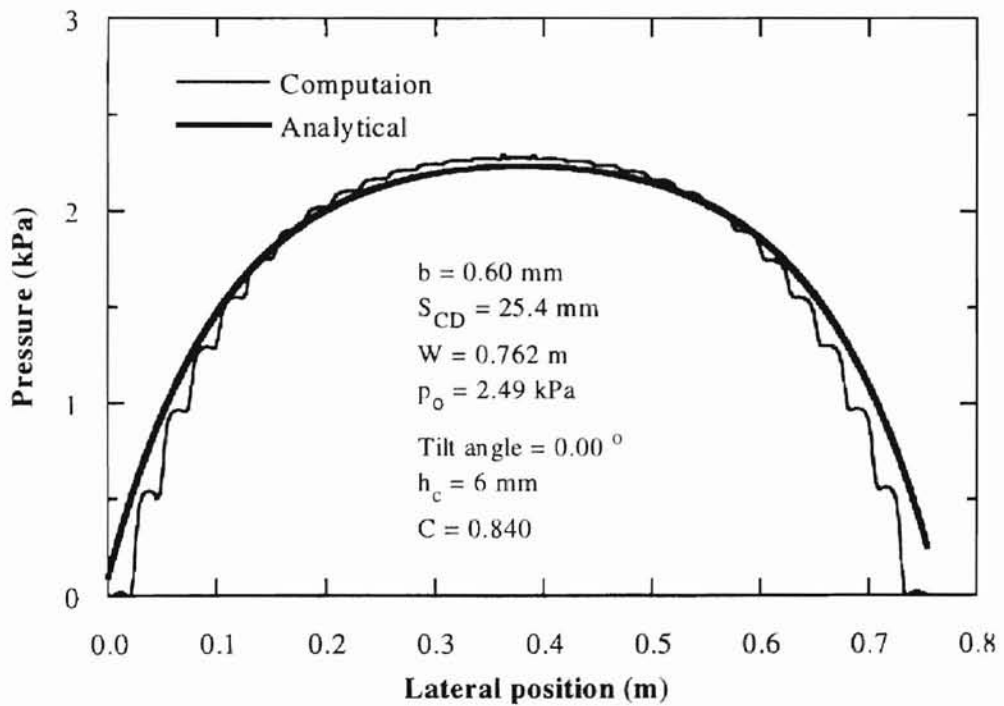


Figure 48. Comparison of Pressure Profiles for $h_c = 6 \text{ mm}$ and $C = 0.840$

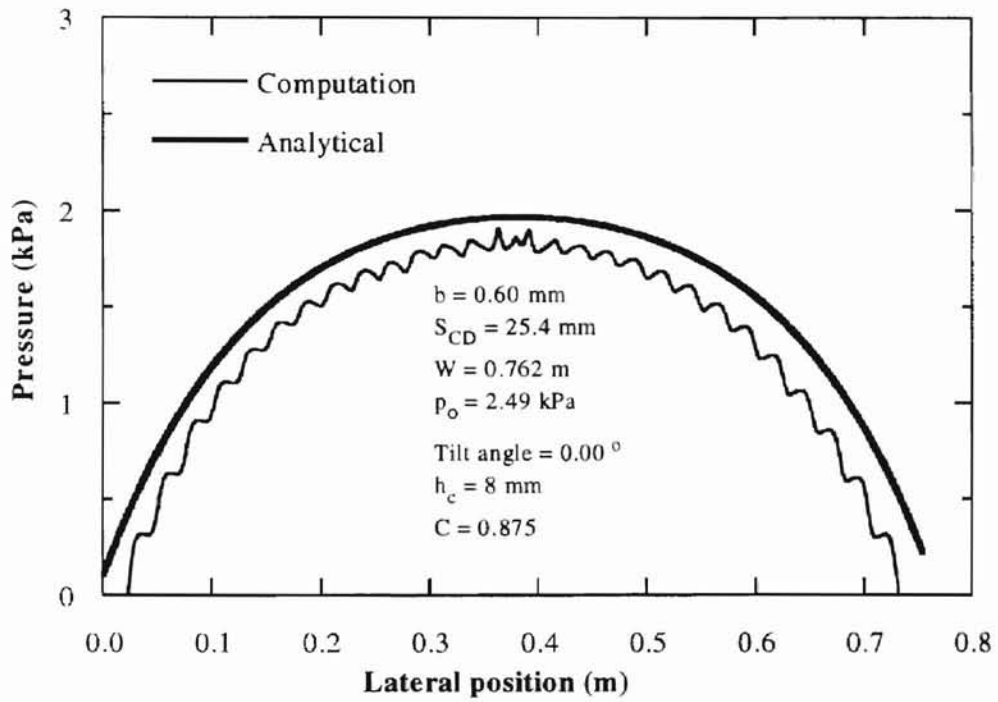


Figure 49. Comparison of Pressure Profiles for $h_c = 8$ mm and $C = 0.875$

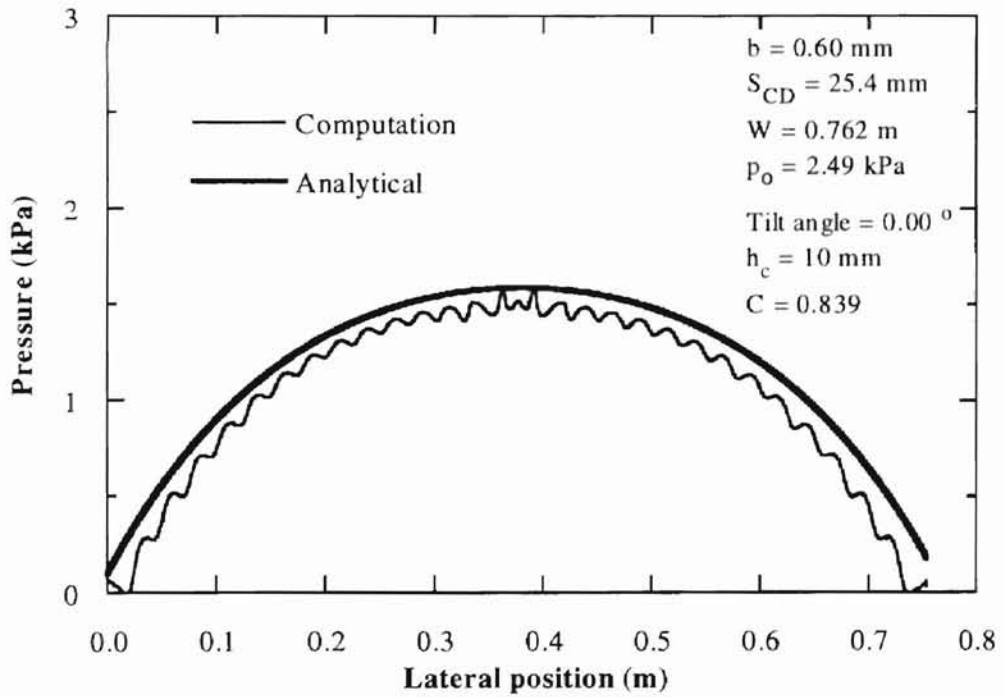


Figure 50. Comparison of Pressure Profiles for $h_c = 10$ mm and $C = 0.839$

CHAPTER 5

CONCLUSIONS

The aerodynamics of a non-tilted and tilted web wrapping over an air reverser was analyzed computationally. The computational model includes the effects of air compressibility and viscosity. The effects of important design parameters such as tilt angle of the web and flotation height were examined. The range of variables is shown in Table 1. The computational results were compared with the analytical model developed by Chang (October 2000). The following conclusions were obtained based on the current computational study:

- The effect of tilt angle on lift force is negligible for small tilt angles.
- The lateral force on a tilted web due to aerodynamic pressure is dominant, and the effect of aerodynamic friction on the lateral force is negligible.
- The lateral force on the tilted web can be obtained by $F_y = F \sin(\beta)$ where the lift force F for a non-tilted web can be predicted.
- When the web is tilted, cushion pressure near the left edge (with smaller flotation height) is higher than that near the right edge.
- The cushion pressure decreases with the increase of flotation height.
- The cushion pressure increases with the tilt angle.

- The maximum pressure for a tilted web is higher than the maximum pressure for a non-tilted web, when all conditions, including the average floatation height, are the same.
- The lift force decreases with the increase of floatation height.
- The lateral aerodynamic force (due to pressure) increases with the tilt angle.
- The lateral aerodynamic force decreases with the increase of floatation height.
- Discharge coefficient changes with floatation height.

CHAPTER 6

RECOMMENDATIONS FOR FUTURE STUDY

It is recommended to extend the computational study as follows:

- Experimentally verify the computational results.
- Conduct a three-dimensional computational analysis.
- Include the effect of flexible web, and obtain solutions that satisfy both fluid dynamics and web deflection equation.
- Conduct more detailed study of discharge coefficient for a variety of test conditions.

REFERENCES

- Barlow, E. J., 1967, "Derivation of Governing Equations for Self Acting Foil Bearing," *ASME Journal of Lubrication Technology*, pp. 334-340.
- Benson, R. C. and D'errico, J. R., 1991, "The Deflection of an Elastic Web Wrapped Around a Surface of Revolution," *Mechanics of Structures and Machines*, Vol.19, pp. 467-486.
- Benson, R. C., 1993, "The Interfacial Mechanics of a Tape Wrapped Around a Flexible Bumpy Roll," *Tribology Transactions*, Vol. 36, pp. 375-380.
- Benson, R. C., 1998, "Stiff Elastic Tape Wrapped Onto a Drum," *ASME Journal of Applied Mechanics*, Vol. 65, pp. 870-873.
- Chang, Y. B., October 2000, "Aerodynamic Characteristics of Perforated-Drum Air Reversers," WHRC Project 0000-2, Tab 11.
- Donnell, L. H., 1976, *Beams, Plates and Shells*, New York, McGraw-Hill.
- Frisch-Fay, R., 1962, *Flexible Bars*, London, Butterworths.
- Hwang, C. J. and Liu, J. L., 1989, "Numerical Study of Two-Dimensional Impinging Jet Flowfields," *AIAA Journal*, Vol. 27, No. 7, pp. 841-842.
- Lin, C. C. and Mote, C. D. Jr., 1995, "Equilibrium Displacements and Stress Distribution in a Two-Dimensional, Axially Moving Web Under Transverse Loading," *ASME Journal of Applied Mechanics*, Vol. 62, pp. 772-779.
- Lin, C. C. and Mote, C. D. Jr., 1996, "The Wrinkling of Thin, Flat, Rectangular Webs," *ASME Journal of Applied Mechanics*, Vol. 63, pp. 774-779.
- Muftu, S. and Benson R. C., 1995, "A Study of Cross-Width Variations in the Two-Dimensional Foil Bearing Problem," *ASME Journal of Tribology*, Vol. 118, pp. 407-414.

Muftu, S. and Cole, K. A., 1999, "The Fluid/Structure Interaction in Supporting a Thin Flexible Cylindrical Web with an Air Cushion," *Journal of Fluids and Structures*, Vol. 13, No. 6, pp. 681-691.

Rouse, H., *Elementary Mechanics of Fluids*, 1946, New York, John Wiley & Sons.

Rongen, P. M. J., 1994, "On Numerical Solutions of the Instationary 2D Foil Bearing Problem," *Tribology and Mechanics of Magnetic Recording Systems, Society of Tribologists and Lubrication Engineers*, SP-29, pp.130-138.

Shelton, J. J., 1968, "Lateral Dynamics of a Moving Web," Ph.D. Dissertation, Oklahoma State University, Stillwater, OK.

Shelton, J. J. and Reid, K. N., 1971, "Lateral Dynamics of an Idealized Moving Web," *ASME Journal of Dynamic System, Measurement, and Control*, Vol. 93, No.3, pp. 187-192.

Shelton, J. J. and Reid, K. N., 1971, "Lateral Dynamics of a Real Moving Web," *ASME Journal of Dynamic System, Measurement, and Control*, Vol. 93, No.3, pp. 180-186.

Tannehill, J. C., Anderson, D. A., and Pletcher, R. H., 1997, *Computational Fluid Mechanics and Heat Transfer*, Second Edition, Washington, DC, Taylor & Francis.

Wolfshtein, M., 1970, "Some Solutions of the Plane Turbulent Impinging Jet," *ASME, Journal of Basic Engineering*, Vol. 92D, pp. 915-922.

VITA ²

Halloluwa. K. S. Jayasekara

Candidate for the Degree of

Master of Science

Thesis: A COMPUTATIONAL STUDY OF AERODYNAMICS OF A TILTED WEB
OVER AN AIR REVERSER.

Major Field: Mechanical Engineering

Biographical:

Personal Data: Born in Colombo, Sri Lanka, on May 21, 1973, the daughter of
Sarath Jayasekara and Rani Jayasekara.

Education: Received Bachelor degree in Mechanical Engineering from Oklahoma
State University, May 1999. Completed the requirements for the Master of
Science degree with a major in Mechanical Engineering at Oklahoma State
University in December, 2000